REGISTRATION OF β-CIT DOPAMINE TRANSPORTER SPECT IMAGES

By

ABHINAY DILIP JOSHI

Presented to the Faculty of the Graduate School of

The University of Texas at Arlington in Partial Fulfillment

of the Requirements

for the Degree of

MASTER OF SCIENCE IN BIOMEDICAL ENGINEERING

THE UNIVERSITY OF TEXAS AT ARLINGTON

May 2006

ACKNOWLEDGEMENTS

I would like to thank everyone who has helped me make this thesis possible. I sincerely thank my supervising professor, Dr. Michael D. Devous, Sr. for his invaluable guidance and constant motivation. It is because of his deep involvement in my project that I could make this thesis possible.

I would like to thank my supervising committee consisting of Drs. Frederick. J. Bonte and Dr. Hanli Liu for their interest in my thesis work and for taking their time to serve on my committee. I am grateful to all of the Nuclear Medicine Center members and especially Mr. Tom Harris for his support and assistance.

Above all, I thank my mother, Veena Joshi, and my father, Dilip Joshi, for believing in my abilities, constantly providing the support I needed and being the greatest teachers of my life.

Last, but not least I would also like to thank Ms. Julie Smith for her much needed suggestions during my work tenure at the Nuclear Medicine Center (NMC-UTSW).

April 13, 2006

ABSTRACT

REGISTRATION OF β-CIT DOPAMINE TRANSPORTER SPECT IMAGES

Publication No: _____

Abhinay Dilip Joshi, M.S

The University of Texas at Arlington, 2006

Supervising Professor: Dr. Michael Devous

This work outlines a method for quantification of nigrostriatal dopaminergic neurons by means of SPECT using the cocaine derivative [^{123}I] β-CIT (^{123}I-labelled 2β-carbomethoxy-3β-(4-iodophenyl) tropane (β-CIT)) as a radiotracer which binds with high affinity to the dopamine receptors. It has been validated (1) that the calculation of a simple ratio of specific/non-specific displaceable binding during a period of binding-equilibrium in the striatum about 20 hrs after the administration of a bolus injection of the tracer gives a strong and reliable index of the binding potential of dopamine uptake sites. Previous studies [2] have shown that the dopaminergic deficit in patients with Parkinson's disease (PD) can clearly be visualized and quantified by using the method for calculation of binding potential. In the current study, the data demonstrate that the dopaminergic nerve cell loss in PD (and in other disorders presenting with a

iii

dopaminergic lesion) can be quantified using [^{123}I] beta-CIT and SPECT. Such quantification makes early diagnosis of PD possible.

Also included is a description of the role of neurotransmitters, their effects on brain functions and neurotransmitter imaging techniques. This description is followed by more detailed explanation of various components of a typical functional human brain mapping analysis including image reconstruction, image registration, image standardization and statistical analysis. The advantages and limitations of each component of the analysis are also described in detail to provide the context in which this work was undertaken.

TABLE OF CONTENTS

Chapter

APPENDIX

LIST OF ILLUSTRATIONS

LIST OF TABLES

LIST OF ABBREVIATIONS

1. [^{123}I] β-CIT…………………...............   iodine-123-2β-carbomethoxy-3β–(4-iodophenyl) tropane

2. [^{11}C] β-CIT…….…………………….…   2β–carbomethoxy-3β–{4-iodophenyl} tropane

3. [^{11}C] CFT…………………………….…   (WIN 35,428, 2 beta- carbomethoxy-3 beta- (4-fluorophenyl) tropane)

4. CT…….....…………………………....   Computed Tomography

5. DA…..……………………………….   Dopamine

6. DAT……….………………………….   Dopamine Transporters

7. PD……..…...……………………………   Parkinson's disease

8. ROI………….…………………………...   Region of Interest

9. VOI ……….…………………………..   Volume of Interest

10. MRI……......……………………………   Magnetic Resonance Imaging

11.SPECT………………………………..   Single Photon Emission Computed Tomography

12. PET…………………………………..   Positron Emission Tomography

13. [^{99m}Tc] TRODAT……………………..   [^{99m}Tc][2-[[2[[[3-(4-chloro-phenyl)8-methyl-8-azablcyclo[3.2.1] oct2y-yl]methyl](2-mercaptoethyl)amino] ethyl]-amino]ethane-thiolato(3-)-N2,N2',S2,S2']-oxo-[1R-(exo-exo)])

CHAPTER 1

INTRODUCTION

1.1 Introduction

Parkinson's disease (PD) is a severe and progressive, disabling neurodegenerative disorder globally observed in 1% of the population over the age of 55 years [3], the mean age at which the disease is first diagnosed. One of the most common presenting features is the asymmetric onset of tremor in the affected body part, such as the hand or foot, when otherwise at rest. In addition to tremor, the other "cardinal features" of PD include slowness of movement (bradykinesia), muscle stiffness (rigidity), and loss of balance (postural instability) [4]. Other typical symptoms of PD include loss of normal facial expression, drooling, low volume slurred speech, difficulty swallowing, shuffling, short-steppage gait and inability to initiate gait, or feeling as if the feet are glued to the floor (freezing)[3, 4]. The presence of tremor, rather than gait and balance problems, as the initial or dominant symptom suggests a favorable prognosis indicating a slowly progressive course. [2, 3, 4] Discrimination of these various symptoms is important for determining the correct treatment plan and prognosis. Although the cause of PD is still not completely understood, remarkable progress has been made toward understanding the mechanisms of neuronal cell loss (neurodegeneration). [1, 2]

Degeneration of pigmented cells, most prominent in the substantia nigra pars compacta (part of the midbrain) is the chief pathological features of this disease [4, 5]. These pigmented cells produce dopamine (DA), an important chemical messenger that transmits signals from substantia nigra to another part of the brain called the corpus striatum. When an action potential is received by a cell, dopamine is released and then binds to the pre- and post-synaptic receptors, evoking a series of biological events [2, 3, 4, 5]. Dopamine has selective transporters, dopamine transporters (DAT), in the cell membrane of its presynaptic nerve terminal. This dopamine transporter (DAT) reaccumulates DA released into the synaptic and extraneuronal space, a process known as reuptake, DAT thereby regulates the lifetime of DA in the extracellular space. The dopamine transporter is therefore an important element for the action of dopamine on locomotion, cognition, affect and neuroendocrine functions. Additionally, because transporters are localized on presynaptic terminals they serve as markers of dopamine neurons. During the early clinical phases of PD, declines in DAT binding are generally more pronounced in the contralateral striatum than in the ipsilateral striatum; in the putamen than in the caudate nucleus; and in the posterior putamen than in the anterior putamen [8].

Structural imaging such as computed tomography (CT) and magnetic resonance imaging (MRI) is of limited importance for differentiating parkinsonian syndromes since structural changes are often only evident by the time the disease is advanced. Parkinsonian syndrome can be partially differentiated on the basis of involvement of different components of the dopaminergic system. To monitor the degenerative process

as accurately as possible in longitudinal studies, a brain imaging technique is required that visualizes the striatal dopaminergic innervations. Positron emission tomography (PET) and single photon emission computer tomography (SPECT) techniques now provide unique opportunities for examining these transporters in the human brain in vivo. Various radiotracers or radioligands for imaging of the dopamine transporters by means of PET and SPECT have been introduced. The radioligand should have high affinity and selectivity for the binding site, ability to penetrate the blood brain barrier, and exhibit low non-specific binding to brain tissue. PET has the advantage of more quantitative instrumentation and versatile choice of radionuclides (e.g., ^{11}C and ^{18}F). The dopa decarboxylase activity of nigrostriatal neurons can be measured with [^{18}F]6-flurodopa and dynamic PET [7]. However, this tracer is not ideal because its peripheral metabolites cross the blood brain barrier and must be considered to achieve quantitative assay. SPECT has the advantage of widespread availability of γ-cameras and offers a vivo, non-invasive diagnostic method to detect nigrostriatal nerve terminal lesions with specific ligands of the DAT [2, 7]. Moreover, while PET is a precise and accurate method for quantification of terminal density and clinical monitoring of PD patients, the expense and complication of the technique limits general applicability at this time. Clearly, a radiopharmaceutical suitable for SPECT would have significant advantages.

The proposed method for the quantification of in vivo binding of radiotracer is the specific (striatum)-to-non-specific (occipital lobe or cerebellum) uptake ratio as pseudoequilibrium to determine binding potential [2, 3, 7, 8]. Ligands available for this approach and having appropriate in vivo properties include [^{123}I]β-CIT, [^{11}C]β-CIT,

[^{99m}Tc]TRODAT, [^{123}I]FP-CIT and [^{11}C]CFT [9]. [^{11}C]CFT has excellent imaging properties with PET, but peripheral metabolism of the tracer should be measured in each patient and care must be taken to account for significant levels of non-specific binding [8]. To date the most important tracer used with SPECT for imaging the DAT is β-CIT [2, 7, 8]. This tracer has high affinity for the DAT in the striatum. It also has a protracted period of striatal uptake enabling imaging 14-24 hours postinjection for stable quantitative measures of dopamine transporters. The purpose was to examine the ability of [^{123}I] β-CIT SPECT to discriminate patients with early PD from healthy controls and to investigate the relationship between the binding measures.

1.2 Objective

The objective of this thesis was two-fold: First, quantification of in vivo binding of radiotracer by the specific (striatum)-to-non-specific (occipital lobe or cerebellum) uptake ratio to determine binding potential; and second, to analyze the striatal [^{123}I] β-CIT binding in the PD patients and in normal healthy controls. A template is created from the normalized β-CIT SPECT image, of the DATs in the striatal area (caudate nucleus and putamen) of the normal healthy control subjects. The patient's images were first normalized with the template and then overlaid with the standard VOIs. Standard VOIs (VOIs) were created using the template and included regions for putamen, caudate nucleus and occipital cortex, and the additional VOIs for the entire striatum. The intensity of the overlaid VOIs was then extracted, and was later used to calculate the mean counts per voxel. The ratio of specific to non-specific striatal [^{123}I] β-CIT

4

binding was then calculated, by subtracting the mean of the counts per voxel in the background region by the mean of counts per voxel in the volume of interest and dividing that measure by the mean of counts per voxel in the background region. The occipital cortex was used as the reference region, or a background, because the density of DAT in the occipital cortex is known to be negligible [9].

Various radioligands, such as cocaine analogues and ^{123}I derivatives for SPECT have been studied earlier. SPECT imaging with ^{123}I labeled cocaine analogues such as [^{123}I] FP-CIT, IPT and altropane, revealed a dramatic loss of striatal dopamine transporters in patients with Parkinson's disease with high signal to noise ratios [1,5]. Of these cocaine analogues for SPECT imaging, most experience has been gained with the tracers [^{123}I] FP-CIT and [^{123}I] β-CIT. Importantly, both [^{123}I] FP-CIT and [^{123}I] β-CIT revealed a loss of striatal dopamine transporters in patients with early Parkinson's disease. In addition these techniques revealed bilateral loss of dopamine transporters in patients with hemi-Parkinson's disease. This finding suggests that these techniques are also sensitive enough to detect preclinical Parkinson's disease as well [4]. Furthermore, both of these SPECT techniques allowed for discrimination between patients with Parkinson's disease and healthy control subjects. This clears the sensitive means of the two radiotracers [^{123}I] FP-CIT and [^{123}I] β-CIT in detecting the degeneration of nigrostriatal dopaminergic neurons.

The rest of this thesis is arranged in the following way. Chapter 2 presents a detail explanation of the creation of a template, including image reconstruction, image thresholding and image registration of different formats (e.g. DICOM, ANALYZE and

Interfile 3.2) of the SPECT images using different software. It also explains the standardization of patients SPECT images, the creation of the volume of interest and the extraction of image intensities. Chapter 3 explains the statistical analysis and presents the analytical results obtained. Chapter 4 includes a discussion of the results and limitations of the study. Finally, Chapter 5 details the conclusions and directions for the future work.

CHAPTER 2

METHODS

2.1 Introduction

This chapter presents a detailed explanation of the creation of a brain imaging template from SPECT images from 10 normal healthy subjects, including image reconstruction, image thresholding and image registration of different formats (e.g. DICOM, ANALYZE and Interfile 3.2) using different software such as MATLAB, SPM, MRIcro and XMedCon. It also explains the standardization of patient SPECT images, the creation of the volume of interest and the extraction of image intensities. Image standardization is an important issue while dealing with images of different formats and different modalities.

2.2 Data Acquisition

2.2.1 Subjects

For the present work the data of $[^{123}I]$ β-CIT SPECT images and MRI images are provided by MGI Pharma Inc. Healthy control data was obtained from 10 normal subjects, with a SPECT image for each normal subject and MRI image for just 4 normal subjects. Thus for healthy subjects the data comprises of 10 SPECT images and 4 MRI images. The patient data was obtained from 102 early Parkinson's disease (PD) subjects. Theses data are from a previous clinical trial conducted by Guilford Pharmaceuticals, now owned by MGI Pharma. The healthy controls have one SPECT

study per subject while the PD patients have at least 2 studies per subject (prior to and after 6 months of treatment) Some PD patients had a 3rd SPECT study several months after the conclusion of the treatment trial. Investigators at UT Southwestern are blind to the stage at which scans were obtained for patient subjects, and thus no analyses of treatment effects were undertaken. In total there are 230 SPECT images of the PD patients and a SPECT image for each of the 10 healthy subjects and MRI images for 4 out of 10 healthy subjects.

2.2.2 Data post- processing

All of the data received from MGI Pharma Inc. were the raw projection images acquired from the SPECT camera. The data obtained from the SPECT image is the result of emission which carries relevant information, but the scattering and background effects should be considered as well. Because of these effects of scattering and background radiation the data received from the SPECT camera are the noisy version of the ideal data. The raw images are nothing but this noisy version of the ideal data. The raw images are provided in DICOM format. For processing, these images needed to be reconstructed. The reconstruction was done using the PICKER ODYSSEY system which has reconstruction software running on a UNIX operating system.

2.2.3 Reconstruction

The software performed following steps for reconstruction:

1) Transverse reconstruction-- This step converts the 2-D projection data into 3-D tomographic data and at the same time removes the slices which are above the brain and below the area and not significant for the further processing.

2) 3-D Post-filtering Transverse File-- A low pass filter is used to filter the 3-D images. After filtering based on the appearance of the images (smooth or grainy) the cut-off was either increased or decreased as needed in order to produce a noise free gray scale image.

3) Attenuation Correct 3-d Post-filtered file-- This tool first aligns the A/P axis of the brain with the image array by rotating it if it appears tilted. After choosing the attenuation coefficient, an ellipse is fitted manually. This ellipse is fitted such that it corrects attenuation caused by brain tissues, skull, scalp and hair. For ^{99m}Tc, the attenuation coefficient is 0.11; for ^{123}I it is 0.1, and so the attenuation coefficient for [^{123}I] β-CIT was set to 0.1.

The three steps of reconstruction listed above were performed on SPECT images of 10 healthy subject and 230 PD patients. Each image required 15 minutes for reconstruction. Figure 2.1 below shows one slice of a 3-D SPECT image for a PD patient. The image is displayed in MRIcro after reconstruction.
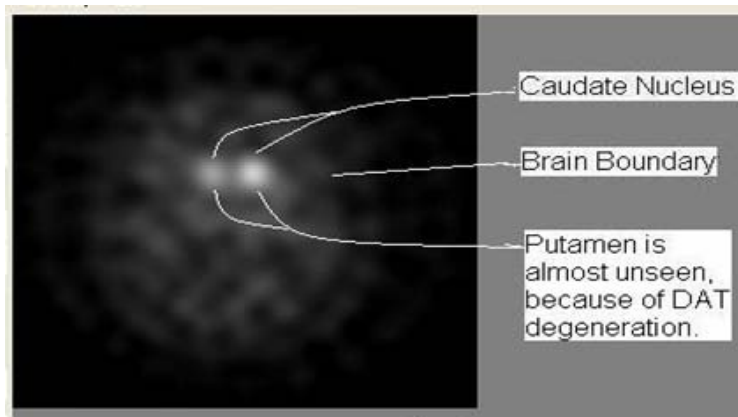
Figure 2.1 A 3-D SPECT image of a PD patient. This image is one slice of SPECT image illustrating the $[^{123}I]$ β-CIT DAT binding in the striatal region.

Figure 2.1 is the SPECT image of a PD patient. In comparison to the image of a normal subject illustrated in Figure 2.2 the degeneration of DAT in the putamen is clearly seen in the patient's image above.
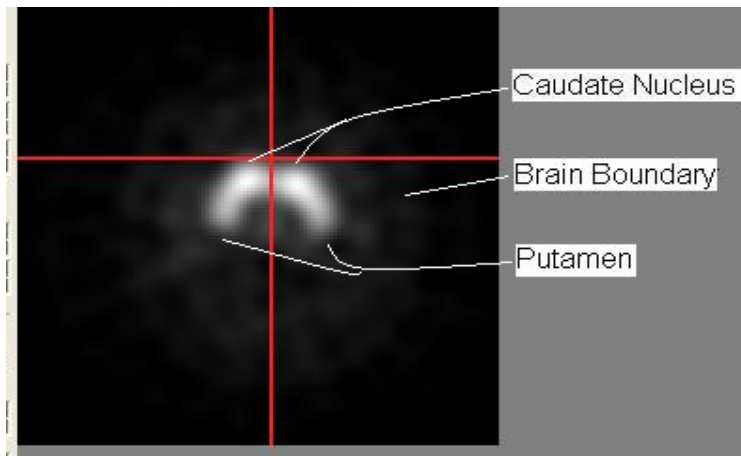
Figure 2.2 A 3-D SPECT image of a healthy control subject. This image is one slice of SPECT image illustrating the $[^{123}I]$ β-CIT DAT binding in the striatal region of healthy control.

2.2.4 MRIcro

MRIcro allows Windows and Linux computers to view medical images. It is a standalone program, but includes tools to complement Statistical Parametric Mapping software (SPM) that allows neuroimagers to analyze MRI, fMRI, SPECT and PET images). MRIcro allows efficient viewing and exporting of brain images. In addition, it allows neuroscientists to identify volumes of interest (VOIs, e.g. lesions). MRIcro can create Analyze format headers for exporting brain images to other platforms.

2.2.5 Fiducial Markers

The reconstructed data is converted into analyze format, which is supported by MRIcro. Each 3-D image has atleast 4 bright regions within each of the 10-15 slices. These bright regions represent anatomical markers, called fiducial markers. Fiducial markers are used when extreme precision is required, such as in the case of image-based surgery, the registration can be based on external fiducial markers, visible in both imaging modalities. They are implanted specifically on the temple and above. Fiducial marker options include the use of anatomic landmarks and extrinsic landmarks. Examples of anatomical landmarks are the tip of the nose, the nasion and tragus [10] or distinct points along the orbital rims [12]. However, precisely and accurately locating an anatomic landmark is difficult because no anatomic feature is sufficiently well defined as a discrete location across subjects. Extrinsic landmarks may be small beads glued to the surface of the skin, or surgical staples. Many of the data sets provided by MGI Pharma contained fiducial markers in the first 10-15 image slices, while the next 15-20

image slices show the β-CIT binding in the striatal regions, mainly caudate nucleus and putamen.

The role of fiducial markers is to provide landmarks that are visible in various image sets from the same subject (e.g., SPECT and MRI) or that indicate the same anatomic location across subjects for the purpose of registering images to as common spatial coordinate system. But there are some disadvantages of having a fiducial marker in the images. Often their intensity is a greater than the intensity of the radioligand. This creates a problem for image registration as registration algorithm can consider this as a control point and perform registration based on this control point. Thus gives an error while registering for the β-CIT DAT binding. Some image processing techniques can eliminate these fiducial markers, but the intensity of fiducial markers can be the same as that of the radioligand binding, in such a case these image processing techniques are not that efficient. There is some software which can take care of the fiducial markers by drawing a region around a fiducial marker in the image and deleting that region. The software used in this study is MRIcro* which has an option to draw a region of interest and deleting the selected region. This is a manual technique, as the subject's brains are of variable shapes and sizes and thus, the positioning of the fiducial markers. Figure 2.3 displays a subject SPECT image containing fiducial marker and Figure 2.4 displays same SPECT image   after removing fiducial markers are shown below.
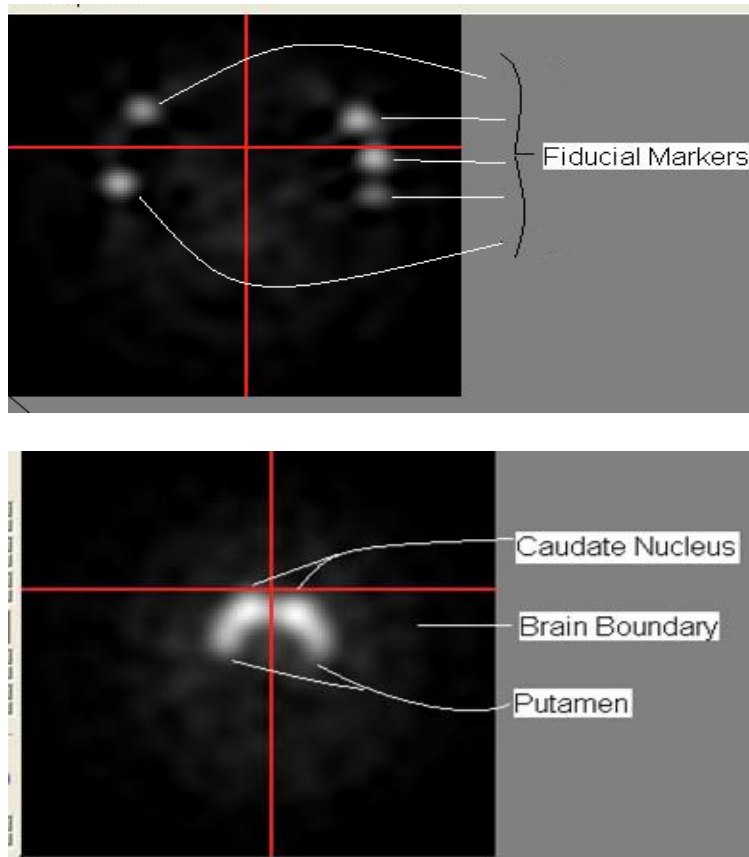
Figure 2.3 A 3-d image showing fiducial markers. There are 5 fiducial markers in the slice number 13 of a SPECT image displayed above. The image below is the 25th slice of the same SPECT image. Fiducial markers appears two light in some slice near the temple region, then keep growing brighter in the next slices and then fade out. In this case the markers are fading out just 2 slices before the slice number 25.
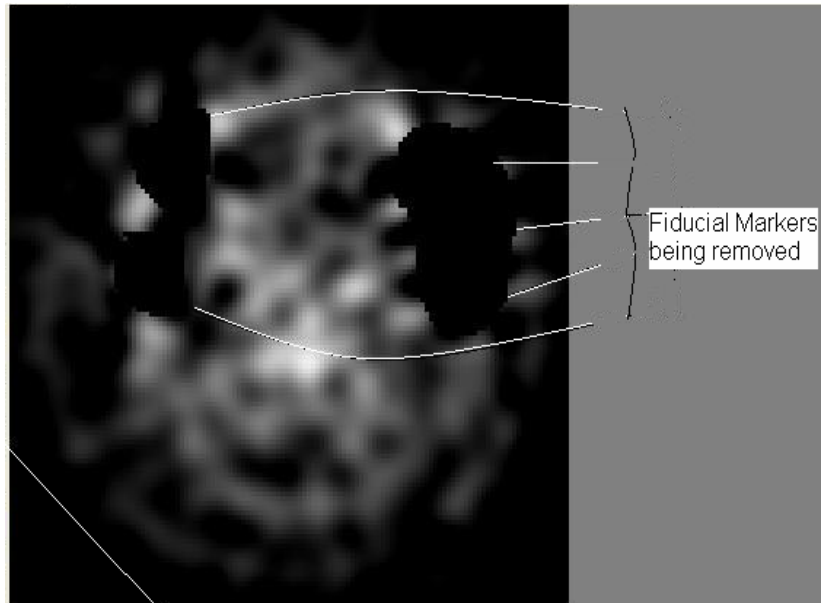
Figure 2.4 A 3-d image with fiducial markers being removed. There are no fiducial markers in the slice number 13. Similarly the fiducial markers from all other image slices are also removed.

As described earlier the SPECT images of normal controls as well as PD patients were

reconstructed and the fiducial markers were removed from them.
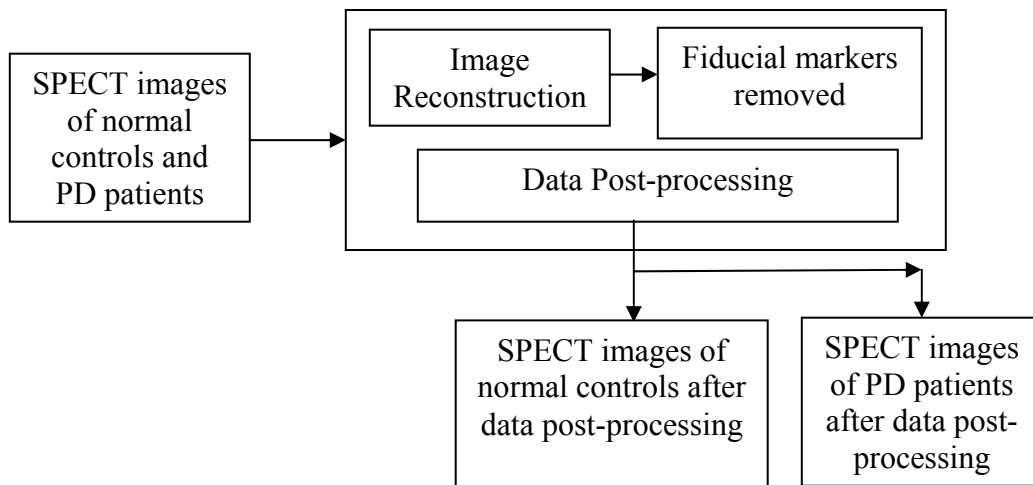
Figure 2.5 The block diagram describing data post-processing performed.

The SPECT images of the normal controls were used to create the template.

2.3 Template Creation

A template is an average of images that contains both specific and non-specific uptake in the standard anatomical/stereotactic atlas. A standard anatomical atlas is a common reference frame used to compare measurements between different subjects and imaging centers. Fox et al 1984 using the principles of anatomical landmark image registration developed a method of locating functional images within a standard space based on the identification of the line through the anterior and posterior commeissures (AC-PC line).
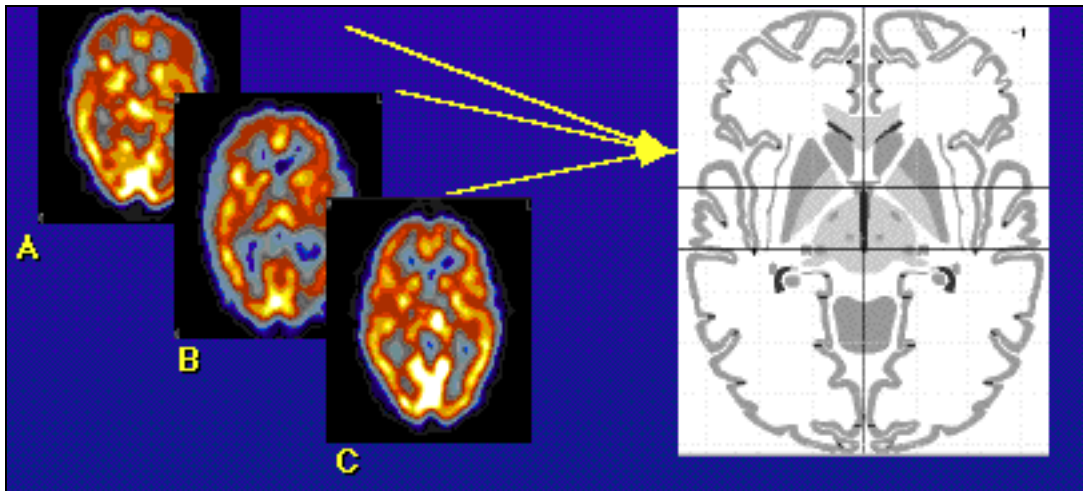
Figure 2.6 Illustrates how a common reference frame can be used to compare functional scans from different subjects.

Template is created from the SPECT and MRI images of the normal controls. The SPECT image provides the functional information and not the structural information. So the SPECT image of a normal control was registered with its respective MRI image, to identify the location of the functional activity. Then the registered functional image is converted to a standard atlas. Averaging the registered SPECT

images provides a reference image which contains both specific and non-specific uptake. An average image represents the variability (both functional and structural) of different normal controls. So, instead of using a separate MRI image for the structural information, a functional image can be registered with the template, which is in a standard structural frame. Thus a two step procedure, 1) registering the functional image with the structural image to mark the location of functional anatomy and 2) converting the registered image to a standard atlas is reduce to just one step, which is registering the functional image with the template in a standard atlas. Moreover MRI image is not required for the structural information. Till now it is very evident that image registration technique is a key to template creation. A very crude definition of registration is overlapping two images of the same scene .A detailed explanation of image registration is provided in the following topics.

As mentioned earlier the MRI images were provided for only 4 normal controls. So an intermediate template was created from 4 normal controls. The block diagram illustrated in the Figure 2.6 displays the technique performed to create an intermediate template. Once an intermediate template was created, the SPECT images of other 6 healthy normal controls along with an intermediate template were used to create final template of 10 healthy normal controls. As illustrated in the block diagram of Figure 2.6 below the SPECT images of the 4 normal controls were co-registered with their respective MRI images. After co-registration the SPECT images were transformed to the standard atlas using spatial normalization technique. Both co-registration and spatial normalization technique performs registration of images across modality. But the only

16

difference between these two techniques is, co-registration register images across-modality and within subjects.
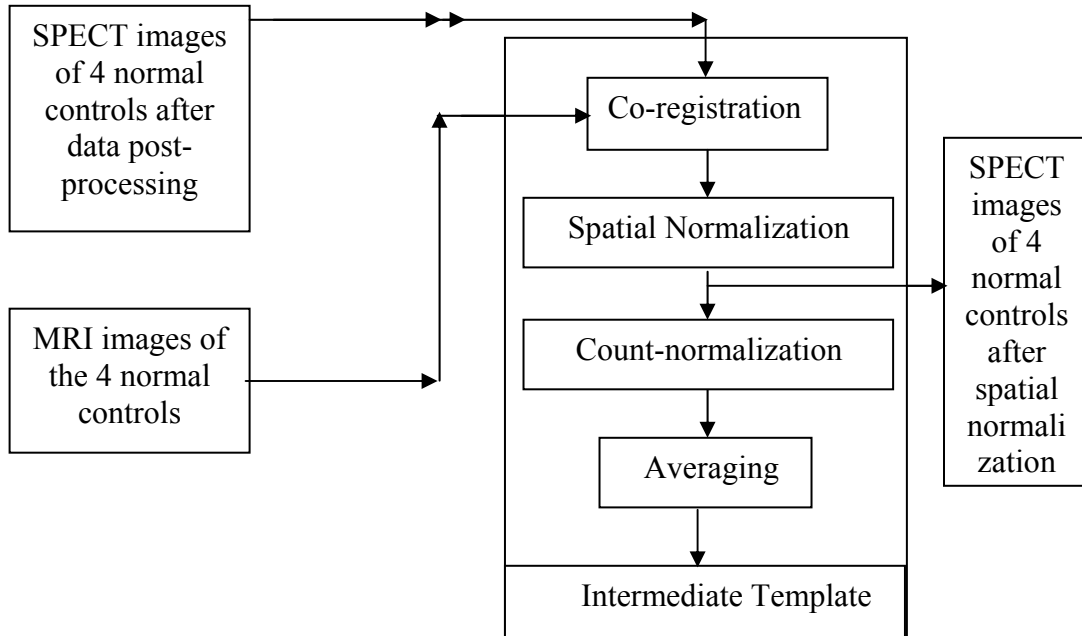
Figure 2.7 The block diagram describing intermediate template creation from 4 healthy normal controls.

And spatial normalization registers images across modality and across subjects. Once the images are spatially normalized, the next step is count normalization, where the intensity counts for each individual are scaled to a comparable magnitude. Once count normalized, the resulting images were averaged to get the intermediate 4 normal controls template, refer block diagram in Figure 2.6.
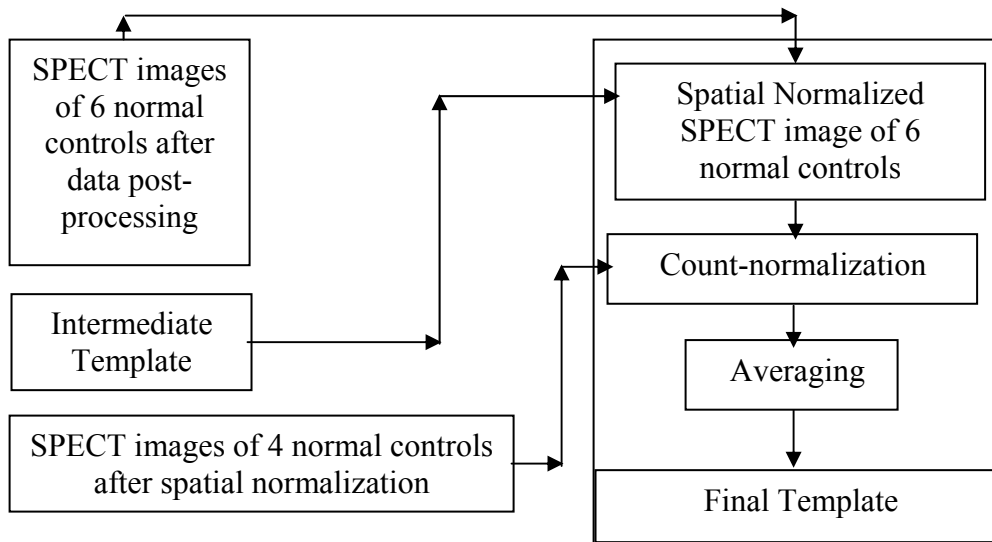
Figure 2.8 The block diagram describing final template creation using the intermediate template and the SPECT images from remaining 6 healthy normal controls.

The intermediate template is an average of SPECT images which was co-registered to an MRI space and then registered to a standard atlas. Refer the block diagram in Figure 2.8 for final template creation. The other 6 normal control SPECT images did not have MRI images. So the only way to locate the functional activity of these images is by using the dimension or the space of the intermediate template. This can be achieved by registering SPECT images of each of the other 6 normal controls with the intermediate template. As this registration was across subjects, a spatial normalization (across subject registration) technique was performed. After spatial normalization the SPECT image of the 6 normal controls were in standard atlas. Now the 6 normal control SPECT images after normalization and 4 normal controls SPECT images after spatial normalization i.e. refer the block diagram of figure 2.7 were count normalized together to get 10 count normalized SPECT images. After count normalization all the SPECT images were averaged to get the final template. The

purpose of the block diagrams was to provide a brief idea of the technique performed to create a template. A detailed explanation of these techniques is provided in further topics. All the techniques shown in the block diagram of Figure 2.6 and Figure 2.7 were performed using Statistical parametric Mapping software (SPM2*).

2.3.1 Statistical Parametric Mapping (SPM2)

SPM2 is generally used to identify functionally specialized brain responses and is the most prevalent approach to characterizing functional neuroanatomy and disease-related changes. As such it is designed for analysing brain imaging data sequence. The sequences can be a series of images collected from different cohorts, or they may be time-series images collected from the same subject.

In order to assign an observed response to a particular brain structure, or cortical area, the data must conform to a known anatomical space. The anatomical spaces supported by SPM are Talairach atlas and MNI atlas. SPM2 has different tools for the realignment of images, spatial normalization, co-registration, count normalization, averaging and for different parametric analyses.

For each tool there is a function written which runs in MATLAB, version 6.5.2. MATLAB version 7.0.4 and & 7.1 does not support all of the aforementioned functions for SPM2, so only MATLAB 6.5.2 is compatible for utilizing all of the functions of SPM2. Each tool in SPM2 supports ANALYZE file format. Therefore all images must be converted to ANALYZE format before SPM2 can be used.

_____

*All tools of SPM2 and MRIcro are included in the Appendix.

2.3.2 Image Registration

Image registration is a technique in which two images of the same scene taken from different modalities, from different angles and at different times are registered together [13]. Image registration is a crucial step in all image analysis tasks in which the final information is gained from the combination of various data sources like in image fusion, change detection and multichannel image registration. Typically, registration is required in remote sensing (multispectral classification, environmental monitoring, change detection, image mosaicing, and weather forecasting, creating super-resolution images, integrating information into geographic information systems (GIS) and in medical imaging to overlay functional and structural images to get more information about the patient [13,15].

According to Jeongate Kim and Jeffery A. Fessler, due to the diversity of images to be registered and due to various types of image degradations it is impossible to design a universal registration method applicable to all tasks. Every registration method should take into account not only the assumed type of geometric deformation between the images but also radiometric deformations and noise corruption, required registration accuracy and application-dependent data characteristics. The majority of the registration methods consist of the following steps, which are illustrated in Figure 2.5 below [13],

1) Feature detection-- Most important and distinctive objects (check-boundary regions, edges, contours, intersections, corners etc.) are manually or preferably, automatically detected. For further processing, these features can be represented by

their point representatives (centers of gravity, line endings, distinctive points) which are referred to as controlled points (CPs) in the literature.

2)   Feature matching-- In this step, the correspondence between the feature detected in the floating image and those detected in the reference image is established. Various feature descriptors and similarity measures along with spatial relationship among the features are used for the purposes of matching features based on the image intensity values in their close neighborhood, the feature spatial distribution or feature symbolic description. Some methods for feature matching include the Correlation-coefficient, Fourier methods and Mutual Optimization

3)   Transform model estimation-- The type and parameters of the so-called mapping functions, aligning the floating image with the reference image are estimated. Some of the mapping functions commonly used includes Similarity transform, affine transform, perspective projection and elastic transform.

4)   Image resampling and transformation-- The sensed image is transformed by means of the mapping functions. Image values in non-integer coordinates are computed by the appropriate interpolation technique.
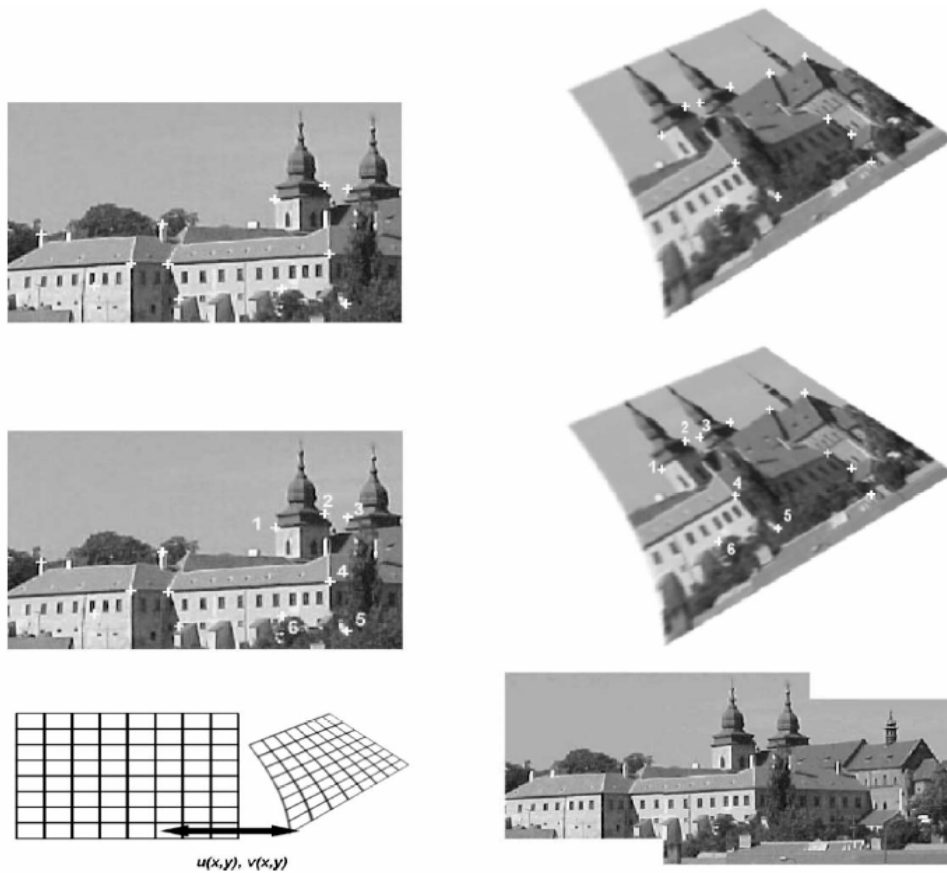
Figure 2.9 Four steps of image registration: top row –feature detection (corners were used as the feature in this case). Middle row-feature matching by invariant descriptors (the corresponding pairs are marked by numbers). Bottom left– transforms model estimation exploiting the established correspondence. Bottom right - shows image resampling and transformations using appropriate interpolation technique [13].

For the registration process, SPM2 supports different feature matching techniques such as, entropy correlation coefficient, mutual information, normalised mutual information, normalised cross correlation. The feature matching technique mutual information is used for this project. Mutual information gives an accurate registration as compared to other techniques.

The transformation method which is used in SPM2 is affine transformation. This transformation considers all of the 12 parameters for the registration in 3-D and 6 parameters for registration in 2-D. Of the 6 parameters for 2-D 2 parameters exist for rotation and 2 parameters for scaling and 2 parameters exist for translation. The SPECT images are 3-Dimensional images, thus 12 parameter affine registration is used. Out of 12 parameters, 3 parameters are for translation and 3 parameters for scaling in x-axis, y-axis and z-axis, and 6 parameters for rotation in x-axis, y-axis and z-axis.

The figures below illustrate the SPECT and MRI image of a normal healthy control subject before co-registration. The SPECT and MRI images are in a different stereotactic space. Through the co-registration process, the SPECT image is brought into the same anatomical space as the MRI image. After registration the SPM2 provides a suffix 'r' to the filename of the earlier SPECT image. In the figure below the z-dimension of MRI image is 60mm, whereas the same dimension of the SPECT image is 49 mm. Once the images are co-registered by using SPM2, all the three dimensions of the co-registered images are aligned with the MRI image. The SPECT and MRI images are properly overlaid so that the SPECT slice number 32 overlays precisely onto the MRI structural image.

Dimension	Size	Origin
X=256	0.94	0.00
Y=256	0.94	0.00
Z=60	3.00	0.00

Dimension	Size	Origin
X=128	2.06	0.00
Y=128	2.06	0.00
Z=49	3.56	0.00
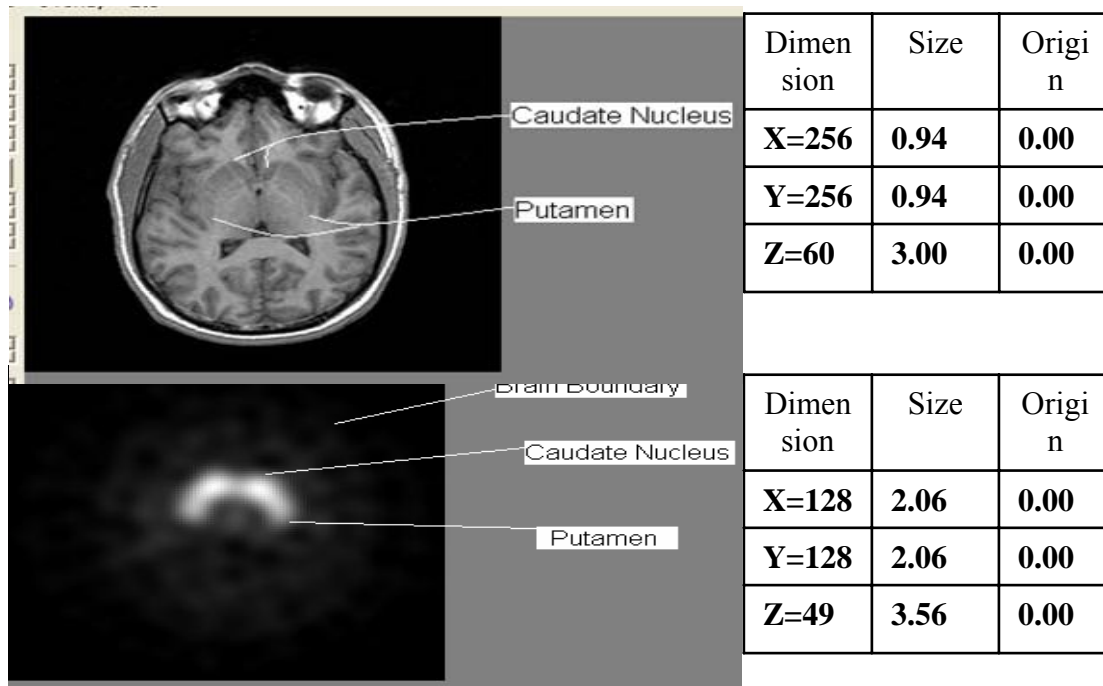
Figure 2.10 MRI image (above) and SPECT image (below) of a normal healthy control subject before co-registration. Check the Dimension, Origin and Size of the MRI image and the SPECT image before co-registration.

Dimension	Size	Origin
X=256	0.94	129.0
Y=256	0.94	129.0
Z=60	0.94	31.00
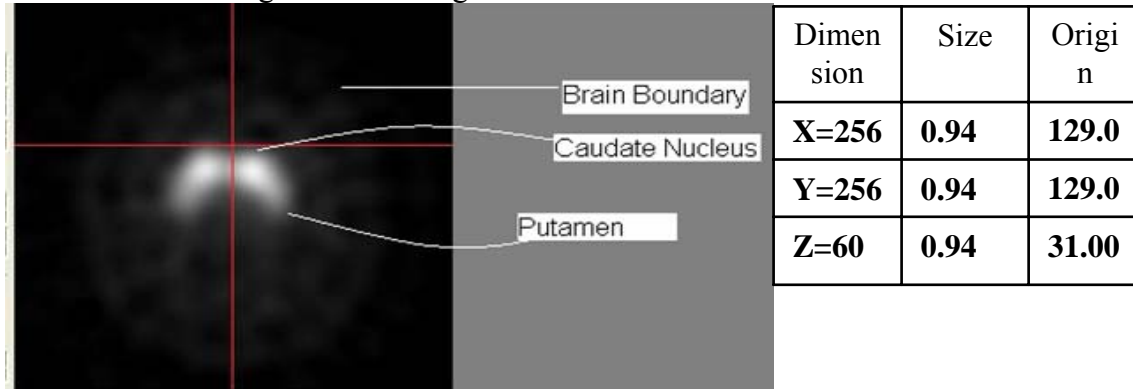
Figure 2.11 This is a SPECT image co-registered with an MRI image of a normal healthy control subject. Check the Dimension, Size and Origin of the SPECT image after co-registration. The SPECT image is converted into the space of the MRI image.

After co-registration the results are checked for the co-registration. A correlation between the brain boundaries, the boundaries of the striatal regions and the center of the caudate nucleus were checked for the MRI image and the registered

SPECT image. As illustrated in the following Figure 2.12 the co-registration results were verified.
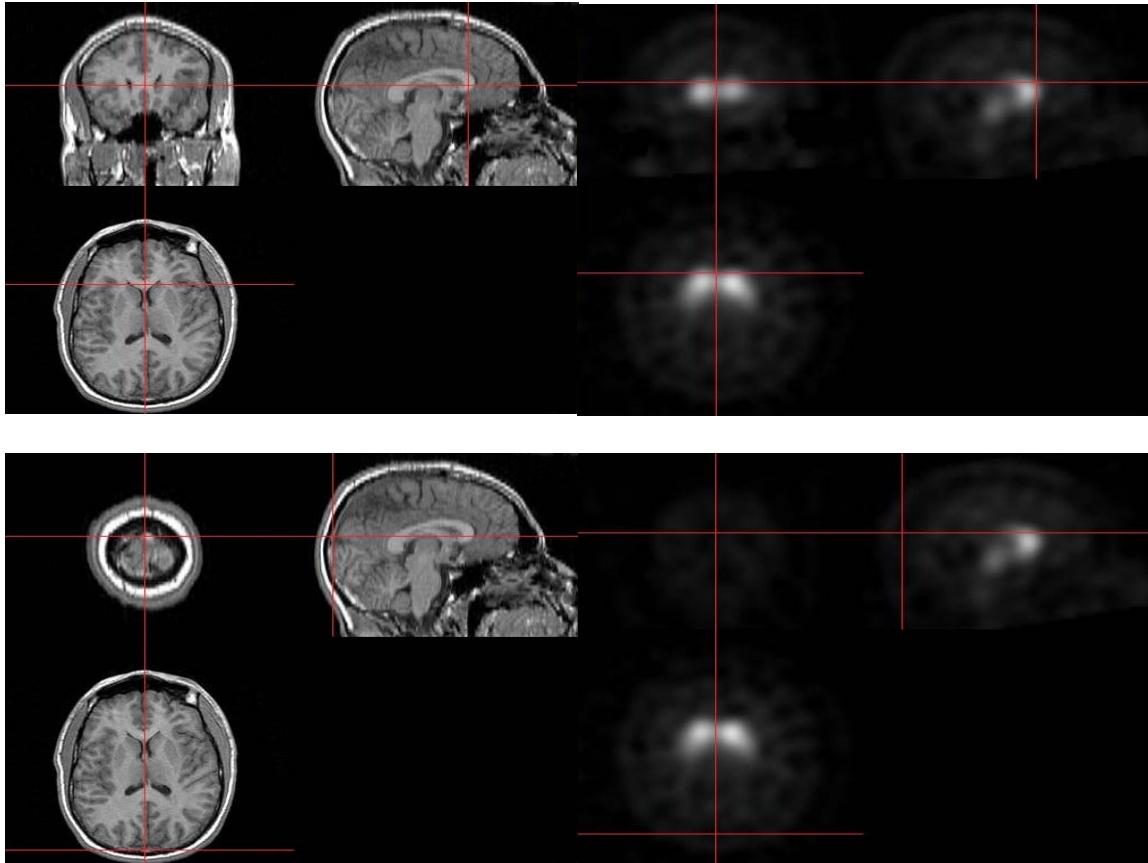
Figure 2.12 Illustrates the measures used to check the result of co-registration of MRI image and SPECT images of healthy subjects.

In the image above the red cross-hairs are arranged on the anterior edge of the caudate nucleus in the MRI image (left) and Co-registered SPECT image (right). In the image below the cross- hairs are arranged at the posterior brain boundary. From visual observation the alignment of cross-hairs are coherent in both the images. Based on alignment of the cross-hairs in the MRI images and co-registered SPECT images the results of co-registration were confirmed.

2.3.3 Spatial Normalization

In the normalization process, a mean image of the series, or some other co-registered image (*e.g.* a T_1-weighted image) is used to estimate some warping parameters that map it onto a template that already conforms to some standard anatomical space (*e.g.* Talairach and MNI). This estimation can use a variety of models for the mapping, including: (i) a 12-parameter affine transformation, where the parameters constitute a spatial transformation matrix, (ii) low frequency basis spatial functions (usually a discrete cosine set or polynomials), where the parameters are the coefficients of the basis functions employed and (ii) a vector field specifying the mapping for each control point (*e.g.* voxel).[Specifically spatial normalization is done for the brains that have gross anatomical pathology, which can be of two sorts [16]:

a) Quantitative changes in the amount of a particular tissue compartment (*e.g.* cortical atrophy): this is not problematic, as changes in the amount of cortical tissue will not affect its optimum spatial location in reference to some templates [16].

b) Qualitative changes in anatomy involving the insertion or deletion of normal tissue compartments (*e.g.* ischemic tissue in stroke or cortical dysplasia): this can introduce substantial error in normalization unless special care is not taken [16].

Actually the SPECT images were first co-registered with the MRI images. So the SPECT image was transferred to the MRI space. After registration the dimension of SPECT image was changed to the dimension of MRI image to match the functional

anatomy with the structural anatomy. The images were spatially normalized with the template to minimize the individual variability. The T1 template is the standard neuroanatomical atlas of the human brain. As the SPECT image is transferred to MRI space after co-registration with the MRI image, so the template to be used for the spatial normalization should be in MRI space which is the template T1. MRI image of a normal control was registered with the T1 template and then that dimension was used a reference. This reference dimension was applied to the SPECT image. That means co-registered SPECT image was registered with image that was obtained from registration of MRI and T1 template. The Figure 2.13 below displays the T1 MNC used to spatially normalize the SPECT image of each normal healthy control. The Figure 2.13 shows the SPECT image after normalization. The x, y and z dimensions of the both images are illustrated.

Dimension	Size	Origin
X=91	2.00	46.00
Y=109	2.00	64.00
Z=91	2.00	37.00
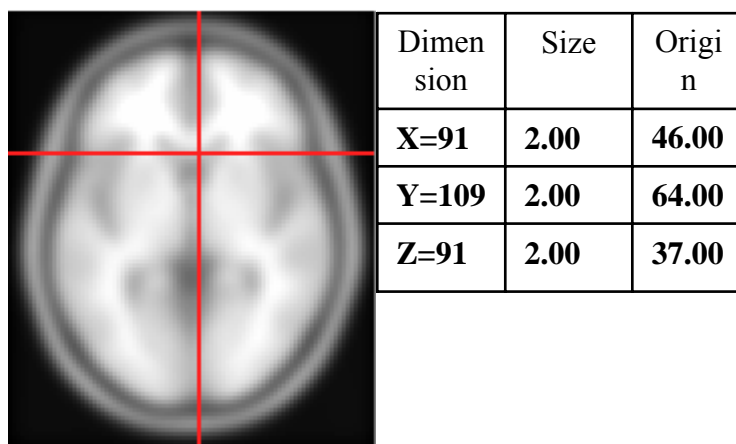
Figure 2.13 Illustrates an image of standard anatomical atlas used to convert the functional images into standard atlas.

Dimen sion	Size	Origi n
X=91	2.00	46.00
Y=109	2.00	64.00
Z=46	4.00	19.00
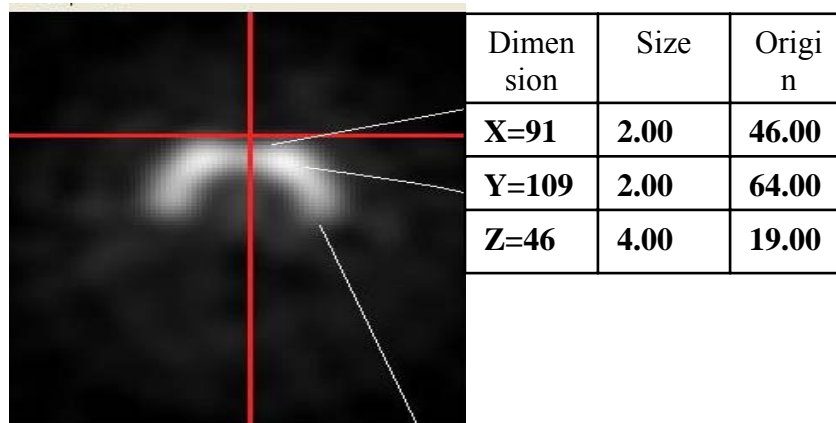
Figure 2.14 A spatially normalized SPECT image of normal healthy control subject.

The Red Cross hairs are arranged at the anterior end of the caudate nucleus.

The spatial normalization results were checked by visual observation of the brain boundaries, boundaries of the striatal regions and the center of the caudate nucleus. Coherence in the alignment of the cross-hairs in spatially normalized MRI image and spatially normalized SPECT image was used as a measure to confirm the results spatially normalization. Figures 2.15 and 2.16 illustrate the check performed to evaluate the results.
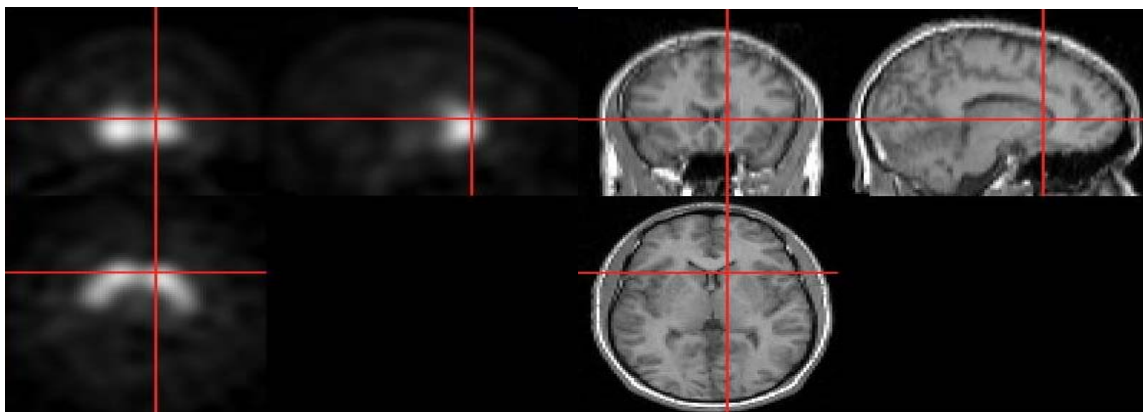
Figure 2.15 Illustrates alignments of cross-hairs in the center of the caudate nucleus in the spatially normalized MRI image and SPECT images.
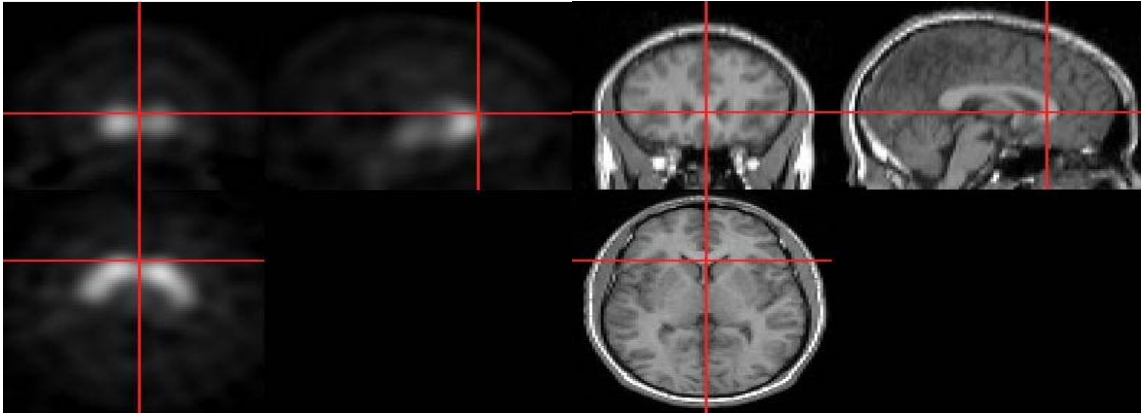
Figure 2.16 Illustrates the visual observation check performed to confirm the results of spatial normalization. The figure illustrates alignment of cross-hairs on the anterior caudate nucleus in the spatially normalized MRI image and SPECT image.

2.3.4 Count Normalization

The radio tracers decay rapidly. The accurate amount of tracer should be injected into each patient. It is also important to control the timing of the radiation measurement scans. Variations in the timing and amount of the radio tracer as well as the subject difference in metabolism and brain activity results difference in the intensity counts within an individual or across subjects. In this case the SPECT images of the 10 healthy subject controls do not have the same contrast range. Therefore, when these images were averaged to get a template, the image with high intensity counts contributed more toward the intensity of the average image and vice versa. So the template was not a true averaged image. To avoid this contrast bias, the images are count normalized, which means the intensity counts for each individual are scaled to a comparable magnitude, which is known as count normalization Count Normalization arranges all the images to same brightness range and contrast range.

29
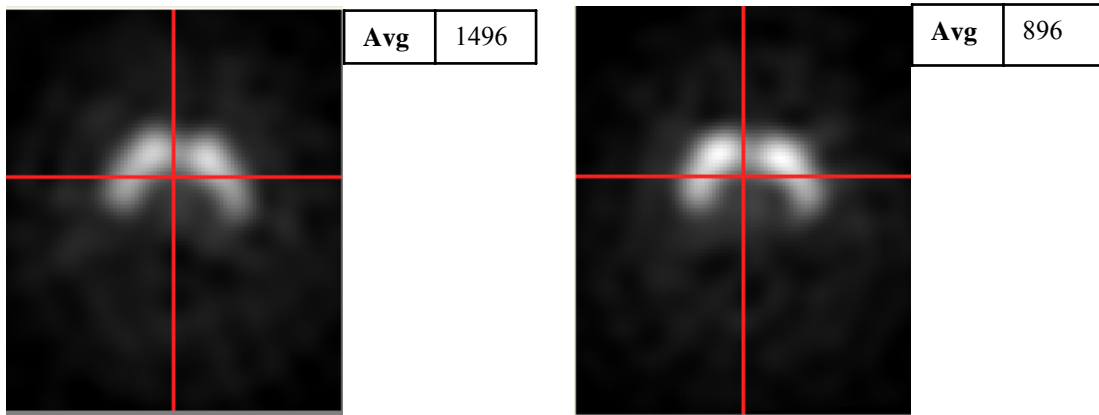
Figure 2.17 The SPECT images of two normal subjects having different intensity range.

SPM2* uses the function *SPM_adjmean_ui** to perform count normalization. Statistical parametric mapping (SPM2) software calculates an average intensity count for a scan using all locations in the rectangular binding box that includes the entire head. Figures 2.17 and 2.18 illustrate the result of using count normalization.
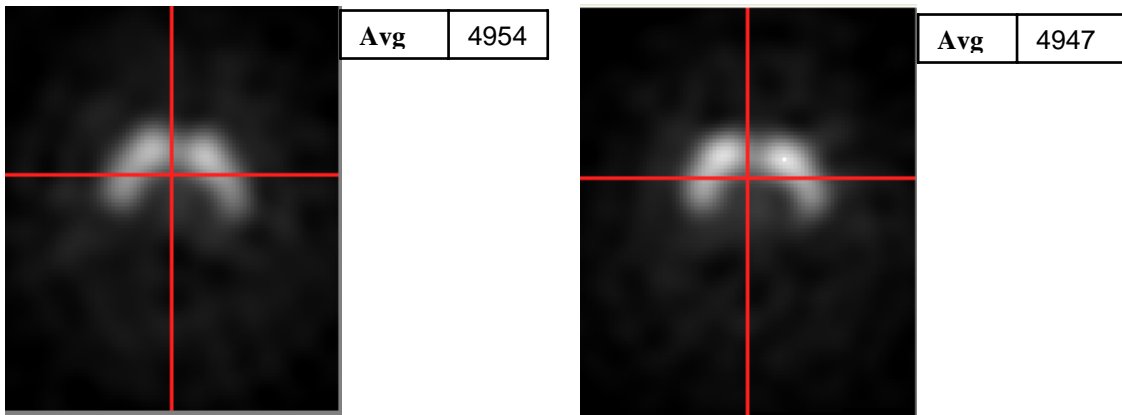
Figure 2.18 The SPECT images of the two healthy normal subjects where the intensity range is arranged to a comparable magnitude.

2.3.5 Averaging

All of the count normalized images are then averaged to create a template. The images are averaged using the function *Imcalc** in SPM2*. This averaged image is nothing but the [^{123}I] β-CIT SPECT template, which is nothing but the averages that contain both specific and non-specific uptake. The Figure 2.19 below displays the average template created from the healthy controls. Dimension, size and the origin is specified in the table displayed in Figure 2.19

Dimension	Size	Origin
X=91	2.00	46.00
Y=09	2.00	64.00
Z=46	4.00	19.00
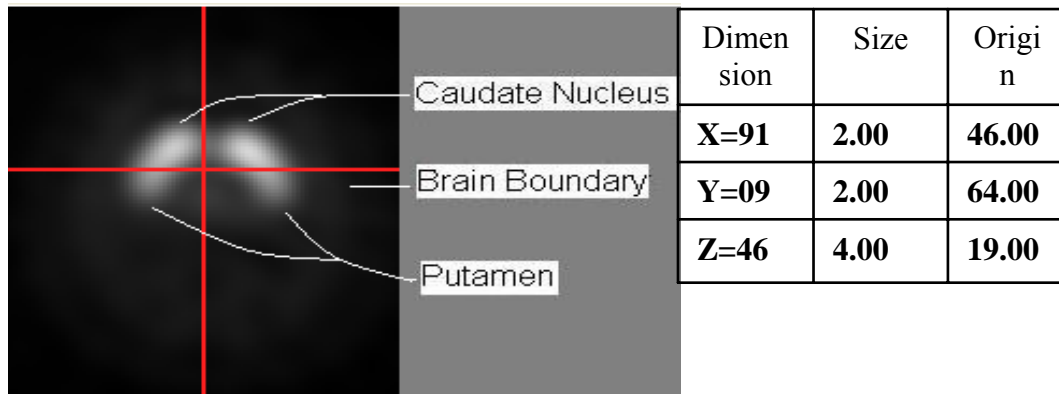
Figure 2.19 The template of [^{123}I] β-CIT SPECT images of 10 healthy normal subjects created after performing co-registration, spatial normalization, count normalization and averaging. Check the Dimension, Size and Origin of this image; these specifications are of the standard anatomical atlas T1.mnc, which was used for the spatial normalization of SPECT images.

The template created above was used to convert all the patient images from this study into a common anatomical space/stereotactic atlas.

2.4 PD patients

For PD patients we were provided with only SPECT images (MRI images were not provided). So, unlike normal healthy controls the PD patient's SPECT images were

not registered with their respective MRI images; but spatially normalized with the template created from 10 healthy normal subject images shown in Figure 2.18.
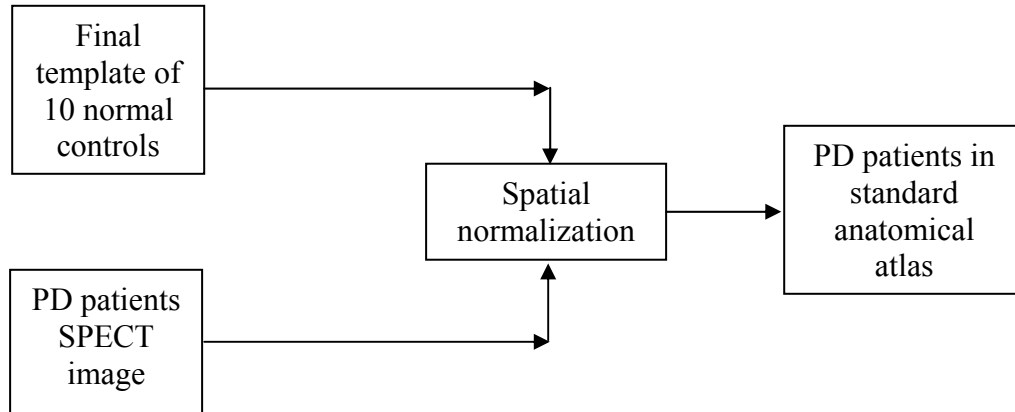
Figure 2.20 Block diagram illustrating the spatial normalization of PD patients using final template of 10 normal controls.

Thus an MRI image is not required for patient; each patient's SPECT image was normalized with the template to reproduce it in a common anatomical space. So, a template created allows the quantitation of the PD patient's without their MRI images. Figure 2.19 below illustrate a patient image before spatial normalization.

Dimen sion	Size	Origi n
X=128	**2.07**	**0.00**
Y=128	**2.07**	**0.00**
Z=50	**3.56**	**0.00**
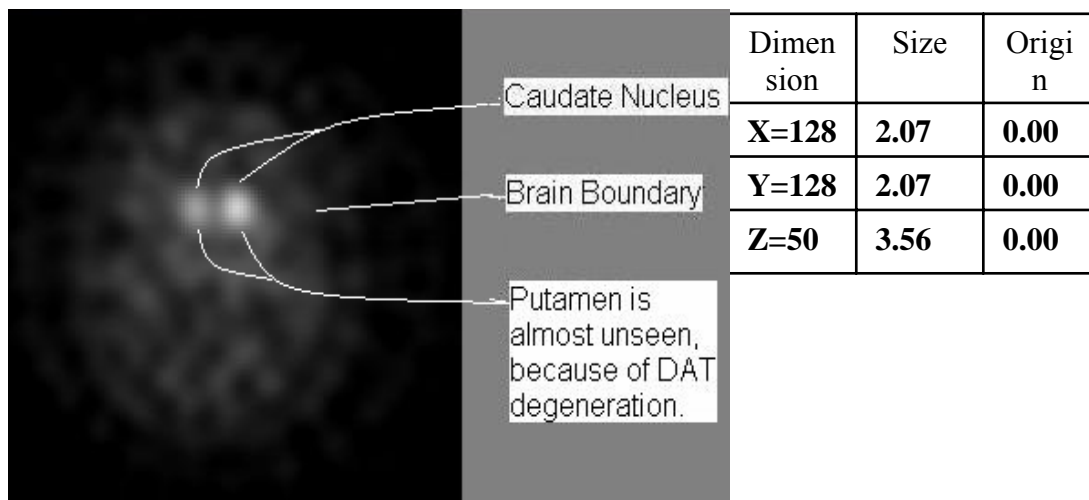
Figure 2.21 A PD patient's SPECT image before spatial normalization. Note the X, Y, and Z values for Dimension, Size and Origin in the upper right corner of the Figure. These values are inconsistent with those provided in normalized images

In the above Figure 2.21 the dimension, origin and size of the image are different from those expected from an image that has been registered in anatomical space. Figure 2.22 below shows the patient image after normalization using [^{123}I] β-CIT SPECT as a template.

Dimension	Size	Origin
X=91	2.00	46.00
Y=109	2.00	64.00
Z=46	4.00	19.00
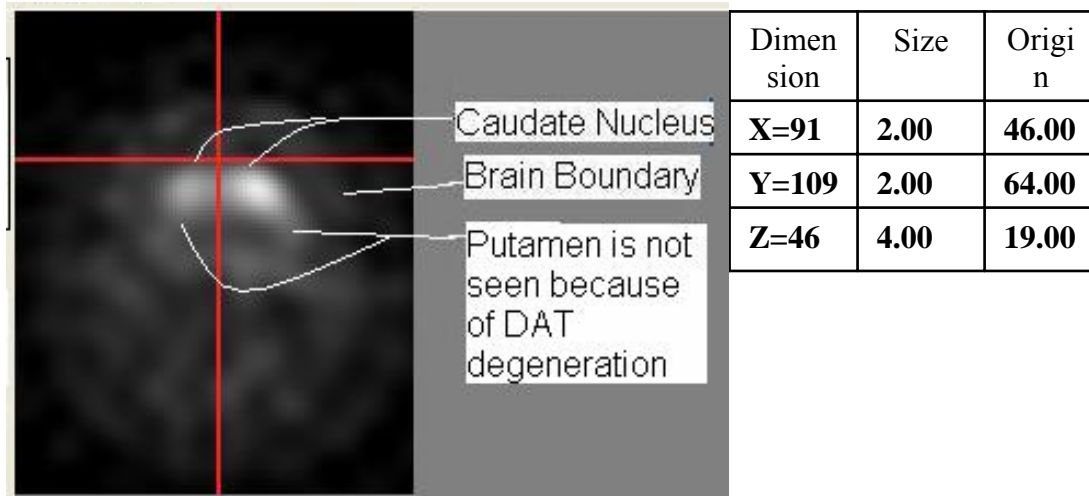
Figure 2.22 A PD patient's SPECT image after spatial normalization. Note the X, Y and Z values for Dimension, Size and Origin in the upper right corner of the figure. These

After normalization, each image is checked for the accuracy of normalization this was done by visual observation of the brain boundaries, the center of caudate nucleus and the boundaries of the caudate nucleus and putamen. Out of 102 patients, 4 patient images were not properly normalized. The reasons behind incorrect normalization are;

1) Incorrect Image acquisition: Some SPECT images are grainy, which is because of incorrect Image acquisition. If a patient moves while image acquisition then the acquired SPECT data will be noisy. In these noisy SPECT images the brain boundaries are not distinguished. Because of incorrect brain boundaries

registration algorithm could not compute the exact overlap which gives improper normalization results.

2) Choosing incorrect bounding box: The bounding box is the dimension which occupies the entire brain. This bounding box is specified in the SPM2 while performing the spatial normalization. If the bounding box is smaller than the dimension of the patients' brain then some of the brain area is clipped thus performing inaccurate normalization.

Out of 102 patients 84 patient images were properly normalized; and the remaining 14 patients' did not have all the images from the SPECT studies they underwent. That means some PD patients' SPECT does not correlate with the number of SPECT studies they had. For some PD patients who had 2 SPECT studies they have only one SPECT image instead of 3 SPECT images i.e. one SPECT image before 1st SPECT study, second SPECT image after 1st SPECT study and third SPECT image for the 2nd SPECT study performed several month after 1st SPECT study . Such patients' were categorized as the one with incomplete SPECT images.

Once the patient images are checked for the accuracy of normalization the images with good normalization were analyzed by overlaying the patients' images with the volume of interest (VOIs).

2.5 Volumes of Interests (VOIs)

The VOIs under consideration are the striatal areas, that are rich in dopamine transporters (DAT), that is, the caudate nucleus and the putamen. These VOIs are of

primary interest because declines in DAT binding are generally more pronounced in putamen in the early clinical phases of PD.

In total, there are 7 VOIs such as, occipital cortex (background), left caudate, right caudate, left posterior putamen and right posterior putamen, left anterior putamen and right anterior putamen. The occipital cortex is considered as the background region because the density of DAT in the occipital cortex is known to be negligible in both patients and normal controls [2, 7].

Each VOI is created using MRIcro, SPECT image and the MRI image from the normal healthy controls. As discussed earlier there are 7 VOIs, right caudate nucleus, left caudate nucleus, right anterior putamen, right anterior putamen, left anterior putamen and left posterior putamen. The caudate nucleus is distinguished from the putamen. But degeneration in regions of putamen is studied by dividing the putamen in to two regions anterior putamen and posterior putamen. The anterior cingulated (AC) is used for dividing the putamen into two anterior and posterior sub-regions. The caudate nucleus, anterior putamen and posterior putamen regions for both the left side and right side were then drawn using MRIcro on the MRI image and the SPECT image of the healthy normal controls. The regions were drawn on the MRI image to decide the anatomic boundaries and on the SPECT image to match the functional activity. Using just the VOIs created from MRI is not ideal because the VOI should match the spatial resolution of SPECT as well. So SPECT VOIs were created. While drawing the VOIs at the junction of the two volumes there can be an overlap. For example if the overlap of caudate nucleus overlaps with the VOI of anterior putamen then the volume of the

overlap is included in the caudate nucleus. Thus 10 VOIs from each normal healthy control was created to get one VOI image for each of the 7 volumes. These VOI are stored in the .roi format. This conversion of VOIs in .roi is done using MRIcro. The Figures 2.17 illustrates the average template created from the 10 healthy controls.
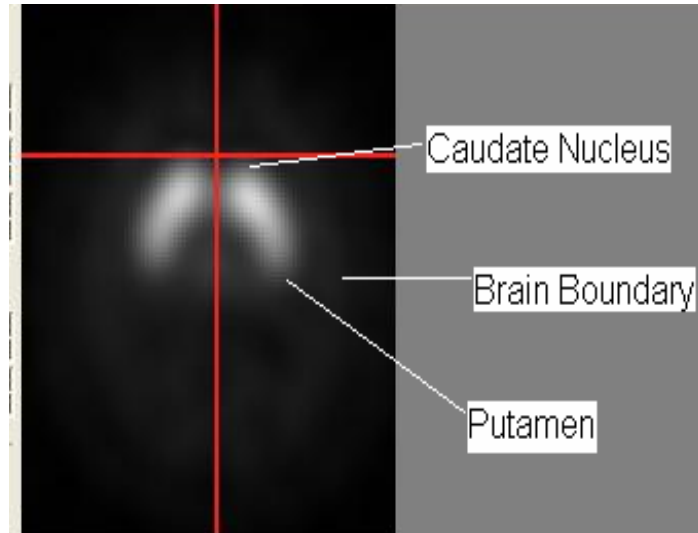
Figure 2.23 The Average template in full range contrast setting displaying the [^{123}I] β-CIT binding in volumes of interest such as putamen and caudate nucleus.
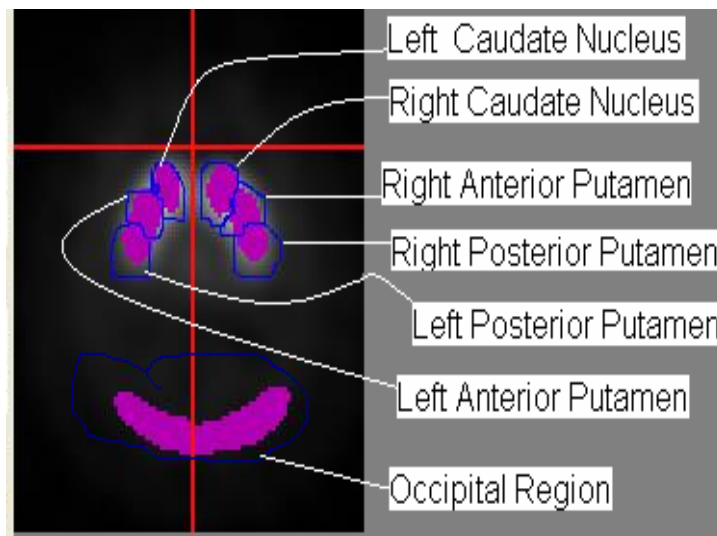
Figure 2.24 The Average template in full range contrast setting overlaid with all the 7 VOIs including background (occipital cortex).

36

In the above Figure for simplicity the template is overlaid with all the volumes of interest. These VOIs were overlaid on each and every patient and then intensity values were extracted in Microsoft Excel. Once the intensity values were extracted from the patients VOI, [^{123}I] β-CIT binding was calculated as the ratio of specific to non-specific [^{123}I] β-CIT binding according to Equation. 1.

$$[^{123}\text{I}] \ \beta\text{-CIT binding} = \frac{VOI - OCC}{OCC} \ \text{-----------------} 1$$

VOI- mean radioactivity in the volume of interest (i.e. putamen and caudate nucleus)

OCC- the mean radioactivity in the occipital cortex

This ratio is called the binding potential which is the product of the maximum available number of receptors and the affinity.

CHAPTER 3

RESULTS AND DISCUSSION

3.1 Results

3.1.1 Spatial Normalization

The normal healthy control SPECT images were spatially normalized to the standard anatomical atlas using the MRI image of respective normal control and the T1 template. The normalizations are tested using the visual observation using the cross hairs in the MRIcro. The cross hairs were placed in the center of the caudate nucleus in the transverse region and then its location is checked with respect to the coronal and the sagittal view. Similarly, if the cross hairs are arranged at the top edge of the caudate nucleus in the transverse region then the cross hairs in the coronal view and in the sagittal view should be aligned at the top edge of the caudate nucleus. Similar results should be observed for the brain boundaries and for the boundaries of the putamen and the caudate nucleus. The Figure 3.1 illustrates a spatially normalized image of the normal healthy control. The image contains the cross hairs arranged at the top edge of the caudate nucleus; it also contains the cross hairs arranged at the center of the caudate nucleus. Using the $[^{123}I]$ β-CIT SPECT template, the PD patient's images were normalized. The Figure 3.2 displays a PD SPECT image, even here the accuracy of normalization was checked as per it is done for the normal control.
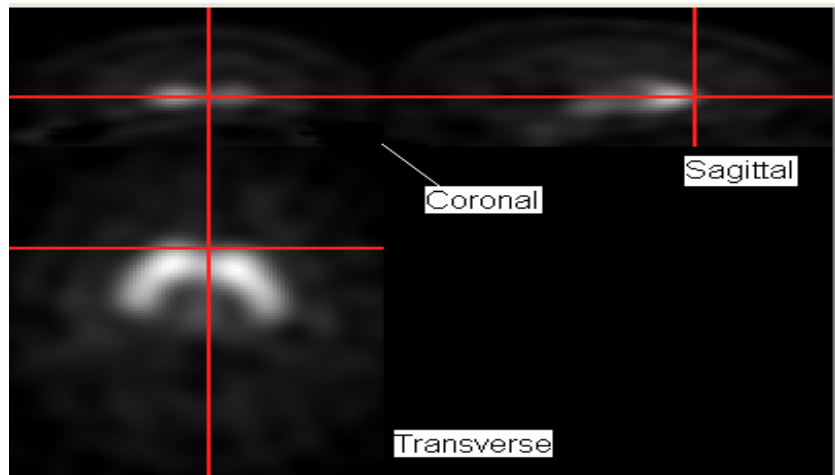
The Cross hairs are arrnged at the top edge of the caudate nucleus, it's seen that the cross hairs in sagittal are aligned at the top anterior end of the caudate nucleus and in coronal view the cross hairs are aligned at the frontal end of the caudate nucleus.
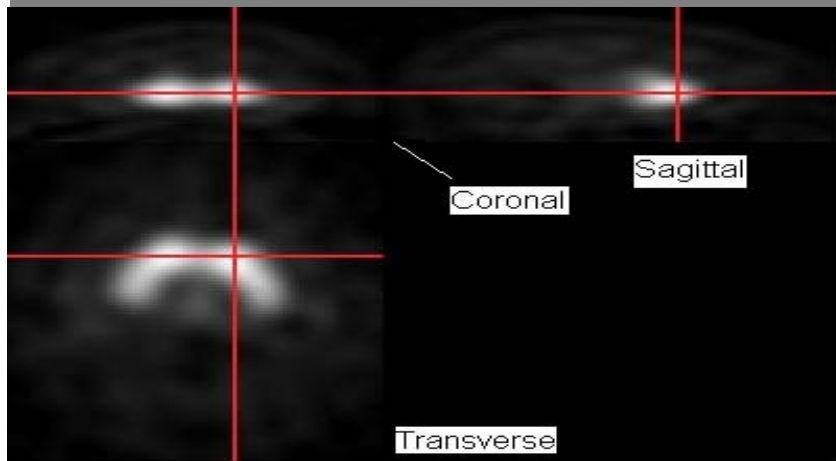
The cross hair is placed at the center of the caudate nucleus, the cross hairs in the sagittal view is also arranged at the center of the caudate nucleus and in coronal view the cross hairs are aligned at the center of caudate nucleus

Figure 3.1 3-D view of the template with cross hairs on the anterior edge of caudate nucleus and at the center of the caudate nucleus. The cross hairs in the coronal view and in the sagittal view are arranged accordingly.

The coss hairs are arranged to the center of the caudate nucleus. The cross hairs are aligned at the center of the coronal and the sagittal view.

The cross hairs are arranged at the top edge of the brain region in transverse view, this aligns the cross hairs at the anterior edge of the brain in the sagittal view
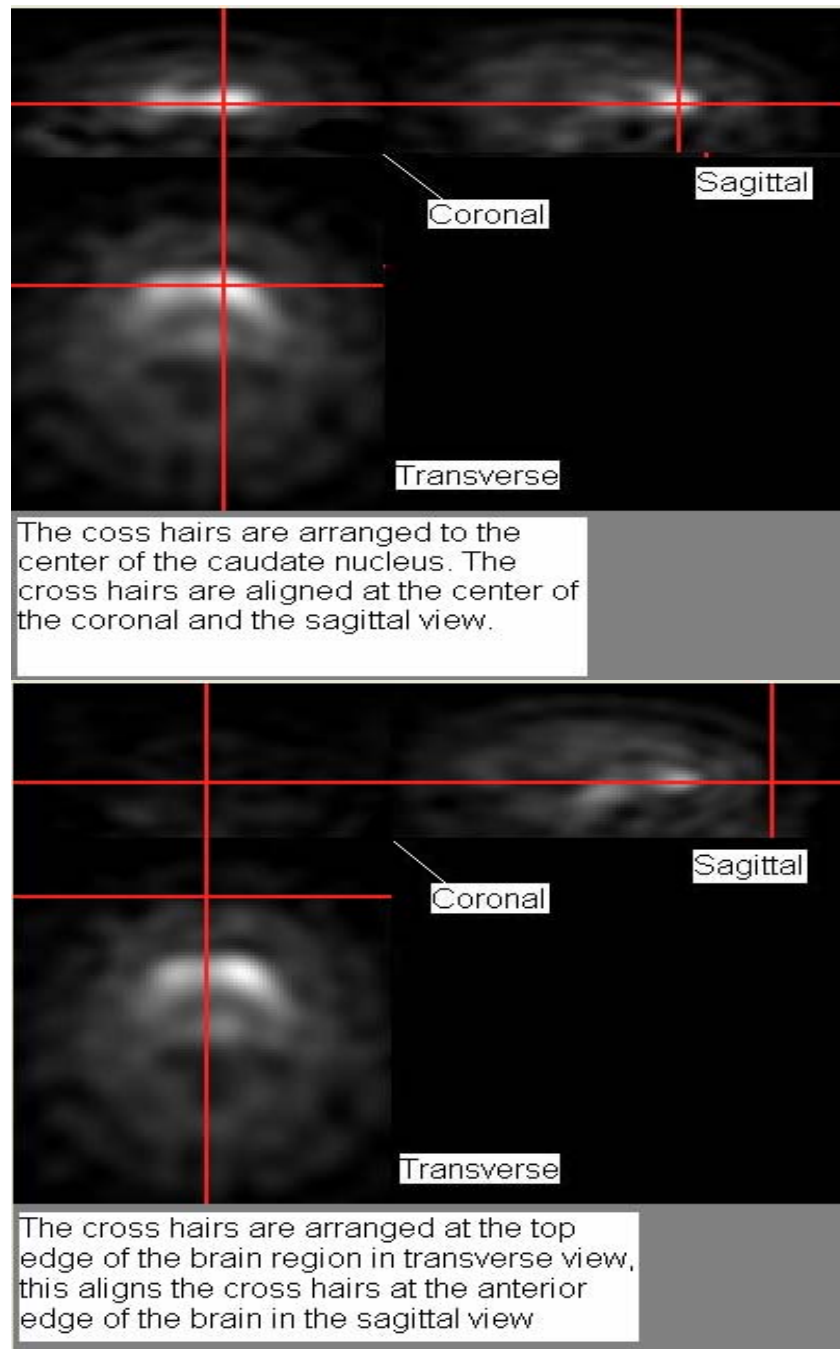
Figure 3.2 3-D view of the spatially normalized patient image. The cross hairs are arranged at the top edge of the caudate nucleus and the top edge of the brain boundary.

In the Figure 3.2 the cross hairs in the coronal and the sagittal view are arranged accordingly. This shows that the normalization is accurate.

40

As compared to the normal healthy controls in PD patients the [123I] β-CIT DAT

binding is not high in the VOIs. Because of this the registration algorithm cannot

register the images based on all the control points which are the VOIs in this case.

There degeneration of DAT in the some VOIs, so in PD patients the registration

algorithm registers the images based on the brain boundaries. This limits the efficiency

of the registration in PD patients' as compared to the normal controls. Also the

normalization of the PD patients is done by tracer specific SPECT template. So if there

is any error in the template, the normalization of the PD patient will get effected and

thus the analysis. If the cross hair in any of the orientation does not align as per their

alignment in other orientations, the normalization result is erroneous. Figure 3.3 shows

the three orientations of PD patients SPECT image which was normalized inaccurately.
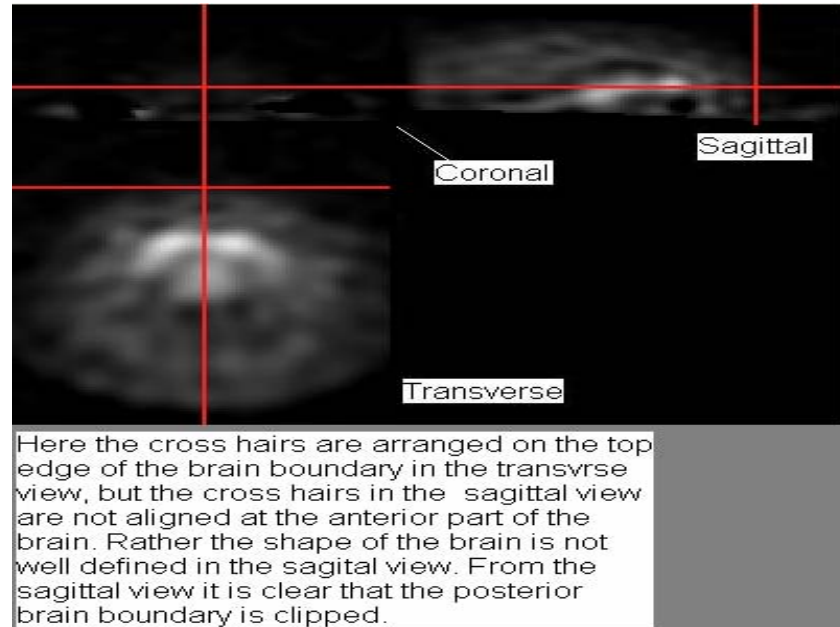
Figure 3.3 The cross hairs are arranged at the top edge of the brain boundary

The cross hair is aligned at the top edge of the caudate nucleus of the brain boundary. But in the sagittal view it can be seen that the cross hair is not arrange at the anteior boundary of the caudate nucleus, rather it is 2 mm apart from anterior edge of the caudate. Also the caudate does not appear in the coronal region.
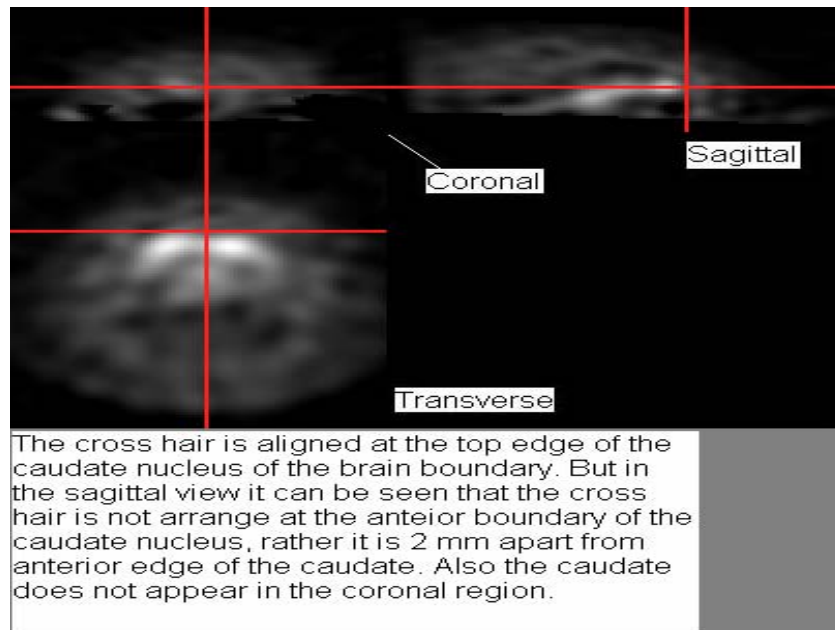
Figure 3.4 The cross hairs are arranged at the top edge of the caudate nucleus.

From Figures 3.3 the brain boundaries are not well defined in the sagittal view. Also the posterior boundary of the brain is clipped to some extent. In Figure 3.4 the cross hair is 2 mm apart from the anterior edge of the caudate nucleus in the sagittal view. Moreover the caudate nucleus should appear in the coronal view but it does not appear in here. From the figures displayed above it could be determined that this patient is not accurately spatially normalized.

3.1.2 VOI Analyses

As spatially normalized SPECT image of a normal healthy control and PD patient is displayed in Figure 3.5 below. For PD patient's analysis the PD patients SPECT image was overlaid with the VOIs to perform the statistical analysis. Some of the patient's image clearly shows the asymmetry in putamen based on the degeneration

of DAT. The visual observation is supported by extracting the values of voxel intensity from a particular VOI and then calculating the uptake ratio from those values. A patient image in the standard anatomical atlas is displayed below.
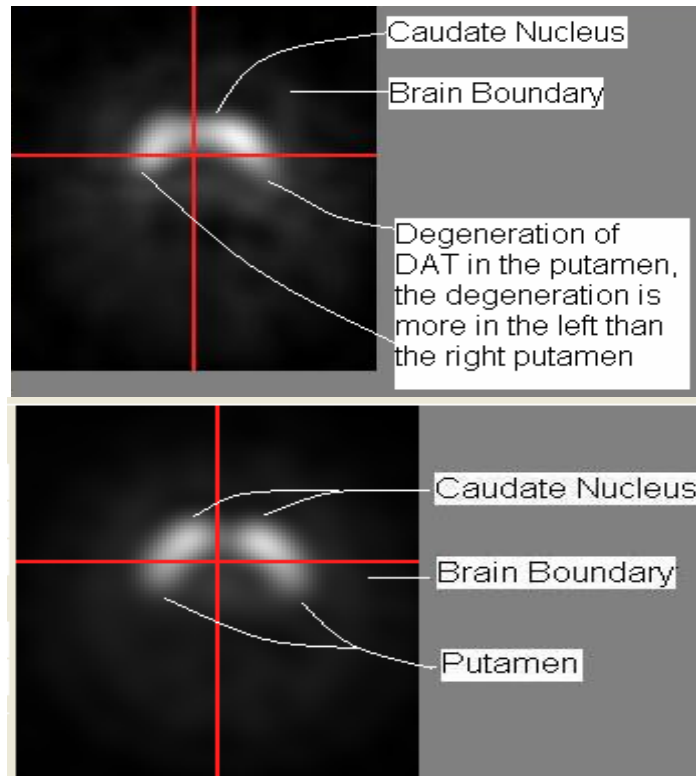
Figure 3.5 A patient's (above) image above when compared with the normal healthy control image (below) depicts the asymmetry in the putamenal region.

3.1.2.1 Background

The Figure 3.6 below displays the background VOI overlaid on a patients image. This VOI was used as a reference for the calculation of the specific binding potential, as the binding of [^{123}I] β-CIT is negligible in this region. The mean intensity value (hereafter abbreviated *occ.)* calculation was computed in the Excel spreadsheet and used for further calculation.
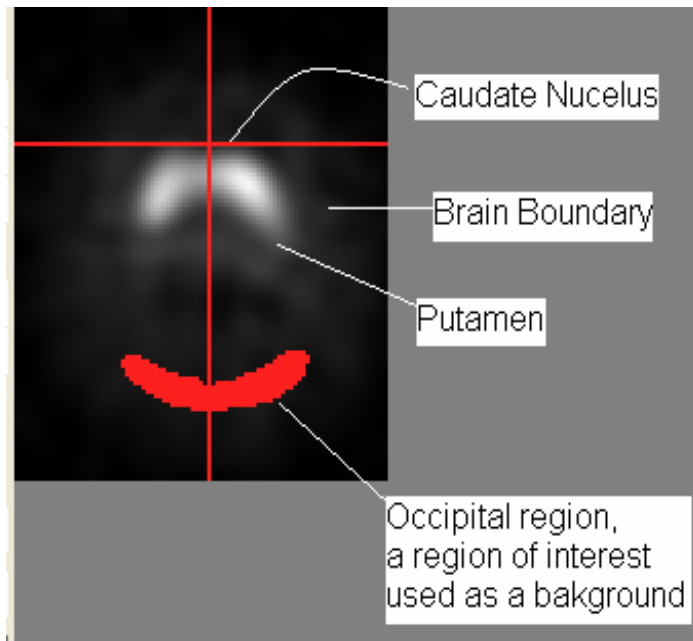
Figure 3.6 Patient image overlaid with occipital region (background) VOI.

The Table 3.1 below displays an Excel spreadsheet containing the dimensions and the voxel intensities is provided. The mean voxel intensity value of the background region (hereafter abbreviated *occ)* is displayed in the Excel spreadsheet below. This value is used further for calculating the value of the uptake ratio of each VOI as illustrated in the Equation. 1 of Methods section.

Table 3.1 The Excel spreadsheet providing the dimension and intensity values of all the voxel from the occipital region of the patient. The first three columns give the x, y, z dimension respectively and the fourth column gives the intensity values. The mean count per voxel is calculated.

X	Y	Z	Intensity Values	Region of Interest
-36	-72	0	300	Occipital
-34	-72	0	306	Occipital
-32	-72	0	312	Occipital
-30	-72	0	318	Occipital
-28	-72	0	324	Occipital
-26	-72	0	328	Occipital
36	-72	0	272	Occipital
38	-72	0	284	Occipital
40	-72	0	287	Occipital
42	-72	0	281	Occipital
44	-72	0	266	Occipital
46	-72	0	245	Occipital
48	-72	0	224	Occipital
50	-72	0	208	Occipital
52	-72	0	201	Occipital
-36	-70	0	297	Occipital
-34	-70	0	307	Occipital
-32	-70	0	317	Occipital
-30	-70	0	328	Occipital
38	-70	0	298	Occipital
40	-70	0	301	Occipital
42	-70	0	296	Occipital
44	-70	0	282	Occipital
46	-70	0	263	Occipital
48	-70	0	245	Occipital
50	-70	0	230	Occipital
52	-70	0	225	Occipital
42	-68	0	318	Occipital
44	-68	0	305	Occipital
46	-68	0	287	Occipital
48	-68	0	270	Occipital
			320.9	**Mean Counts Per Voxel**

3.1.2.2 Left Caudate Nucleus

The Figure 3.7 below displays the overlap of the VOI image of Left caudate nucleus on a patients' image. By visual observation it can be determined that the VOI is exactly overlapped on the patients' left caudate nucleus. In order, to know more about binding potential the mean of the voxel intensities and the uptake ratio were calculated. The mean voxel intensity of occipital region was used to calculate the uptake ratio of each VOI.
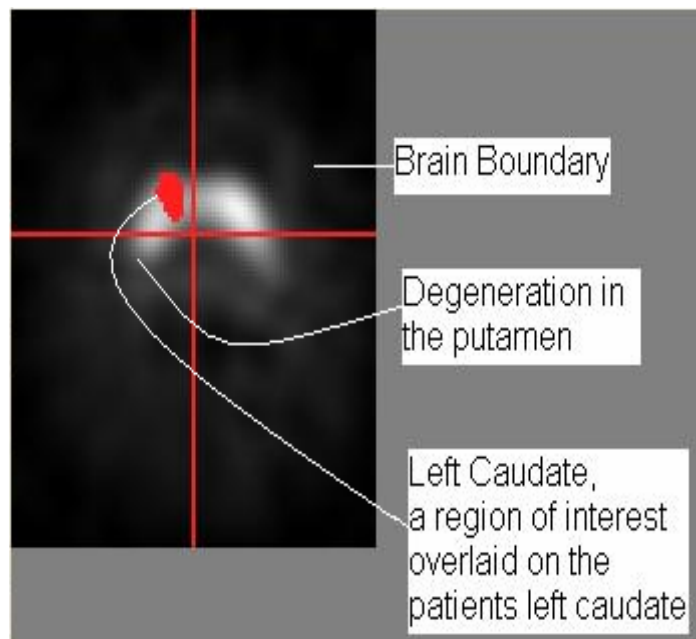
Figure 3.7 A patient's image overlaid with VOI image of Left caudate nucleus.

Table 3.2 The Excel spreadsheet providing the dimension and intensity values of all the voxel from the Left Caudate Nucleus region of the patient. The first three columns give the x, y and z dimensions respectively and the fourth column gives the intensity values. Here the uptake ratio is calculated using the *occ* region described above and equation 1 in the Methods section.

X	Y	Z	Intensity Values	Region Of Interest
-14	14	4	2058	Left caudate nucleus
-12	14	4	2027	Left caudate nucleus
-10	14	4	1971	Left caudate nucleus
-8	14	4	1893	Left caudate nucleus
-6	14	4	1826	Left caudate nucleus
-16	16	4	1852	Left caudate nucleus
-14	16	4	1884	Left caudate nucleus
-12	16	4	1871	Left caudate nucleus
-10	16	4	1826	Left caudate nucleus
-8	16	4	1768	Left caudate nucleus
-6	16	4	1715	Left caudate nucleus
-16	18	4	1628	Left caudate nucleus
-14	18	4	1673	Left caudate nucleus
-12	18	4	1669	Left caudate nucleus
-10	18	4	1636	Left caudate nucleus
-8	18	4	1587	Left caudate nucleus
-14	20	4	1430	Left caudate nucleus
-12	20	4	1439	Left caudate nucleus
-10	20	4	1409	Left caudate nucleus
-8	20	4	1360	Left caudate nucleus
-14	22	4	1184	Left caudate nucleus
-12	22	4	1191	Left caudate nucleus
-10	10	8	1652	Left caudate nucleus
-8	10	8	1579	Left caudate nucleus
-10	12	8	1597	Left caudate nucleus
-8	12	8	1538	Left caudate nucleus
-10	14	8	1498	Left caudate nucleus
-8	14	8	1442	Left caudate nucleus
			1816.0	**Mean Counts per voxel.**
			4.68	**Uptake ratio**

3.1.2.3 Right Caudate Nucleus, Right Anterior Putamen and Right Posterior Putamen

Figure 3.8 below displays the overlap of the VOI image of right caudate nucleus, right anterior putamen and right posterior putamen on the patients' image. This degeneration can be measured by the values of uptake ratio which can be calculated for these VOIs as shown in the Excel spreadsheet in Table 3.2.

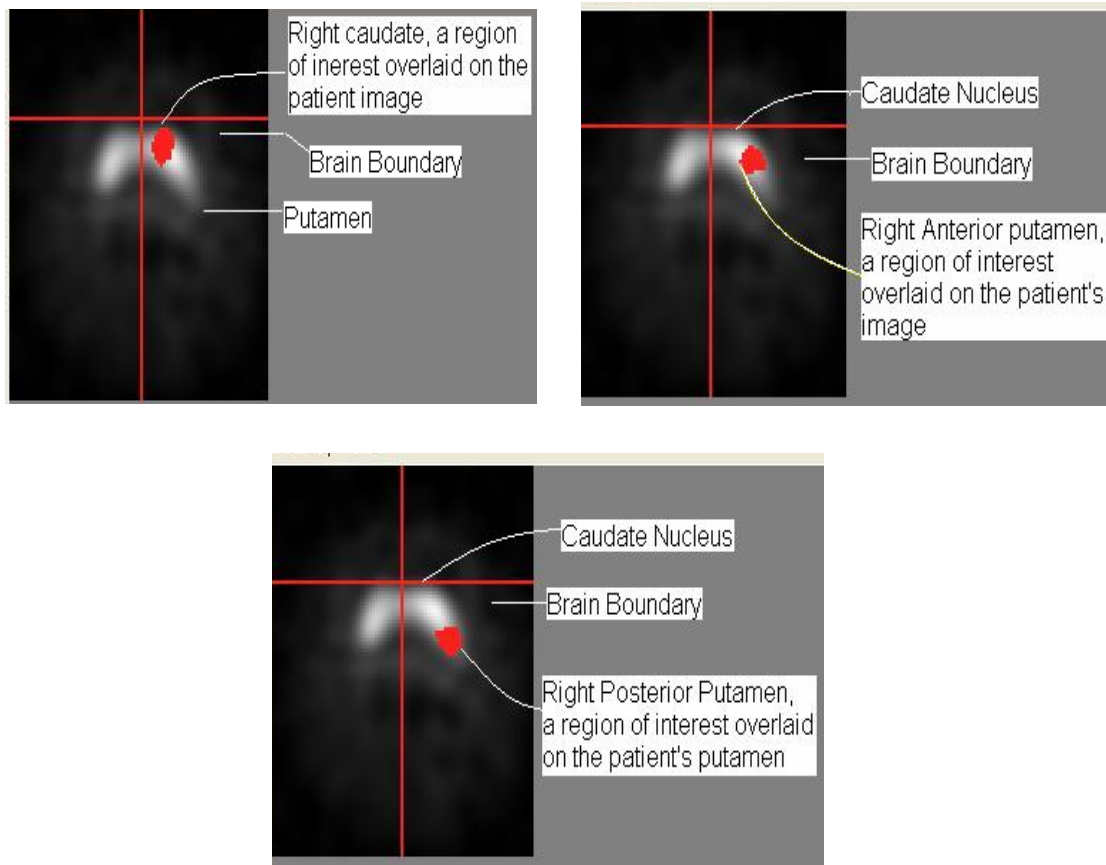**Figure 3.8** A patient's image overlaid with VOI image of Right Caudate nucleus, Right Anterior Putamen and Right Posterior Putamen. The uptake ratios for these overlaps were calculated from the Excel spreadsheet as shown in Table 3.2. The values of uptake ratios for this patient for the Right Caudate nucleus, Right Anterior Putamen, Right Posterior Putamen are **6.04, 5.67, and 3.82** respectively.

3.1.2.4 Left Anterior Putamen and Left Posterior Putamen

The overlay of the VOI image of Left Anterior Putamen on the patient image is illustrated. Comparing the two images below the overlap of the VOI of anterior putamen is better than that of the posterior putamen. The uptake ratios for these VOIs were done similar to the one shown in Excel spreadsheet of the Table 3.2.
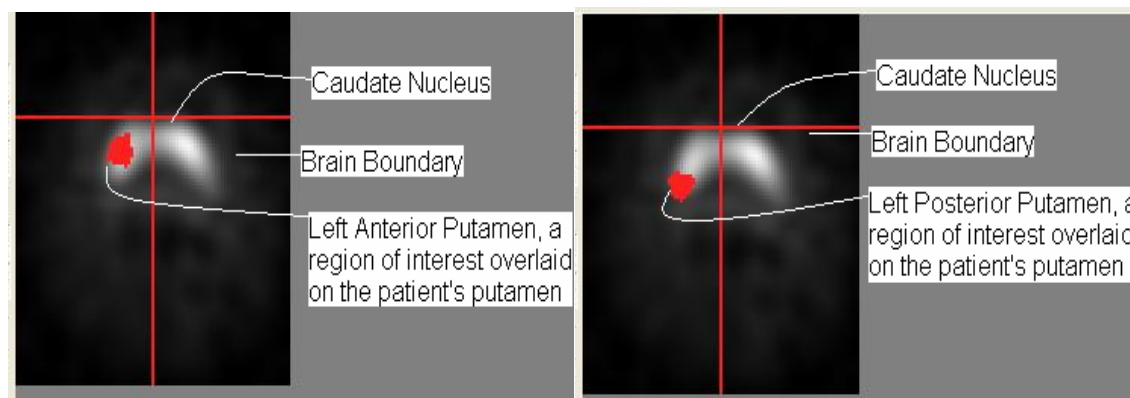
Figure 3.9 A patients' image overlaid with VOI image of the Left Anterior Putamen and Left Posterior Putamen.

3.1.3 Statistical Analyses

As shown above the uptake ratio of radioligand binding for each and every patient was calculated. Plotted below are the graphs of uptake ratio of $[^{123}I]$ β-CIT in the right side of the striatal volumes such as right caudate, right anterior putamen and right posterior putamen. The uptake ratio for the 10 normal healthy control subjects as well as the mean uptake ratio for the 10 healthy controls is also included in the plots below.

Figure 3.10 Uptake Ratio of beta-CIT in Right Caudate Nucleus of 131 Male patients. The Blue color plot is for the mean uptake ratio of 131 male patients, Pink color is for uptake ratios of each male patient and the yellow color is for the uptake ratio of 10 normal healthy control subjects. The mean uptake ratio for 131 male patients is **3.28**. The mean uptake ratio for healthy control is **6.19**.

Table 3.3 This table illustrates the mean uptake ratios values for the right striatal regions

Mean Uptake Ratio	Right Caudate	Right Ant. Putamen	Right Post. Putamen.
10 Healthy Controls	6.19	6.10	4.84
131 Male Patients'	3.28	3.23	2.04
42 Female Patients'	3.93	3.83	2.57

The Table 3.3 above displays the uptake ratio values for the right caudate nucleus, right anterior putamen and right anterior putamen, for 131 male patients', 42 female patients' and 10 healthy controls.
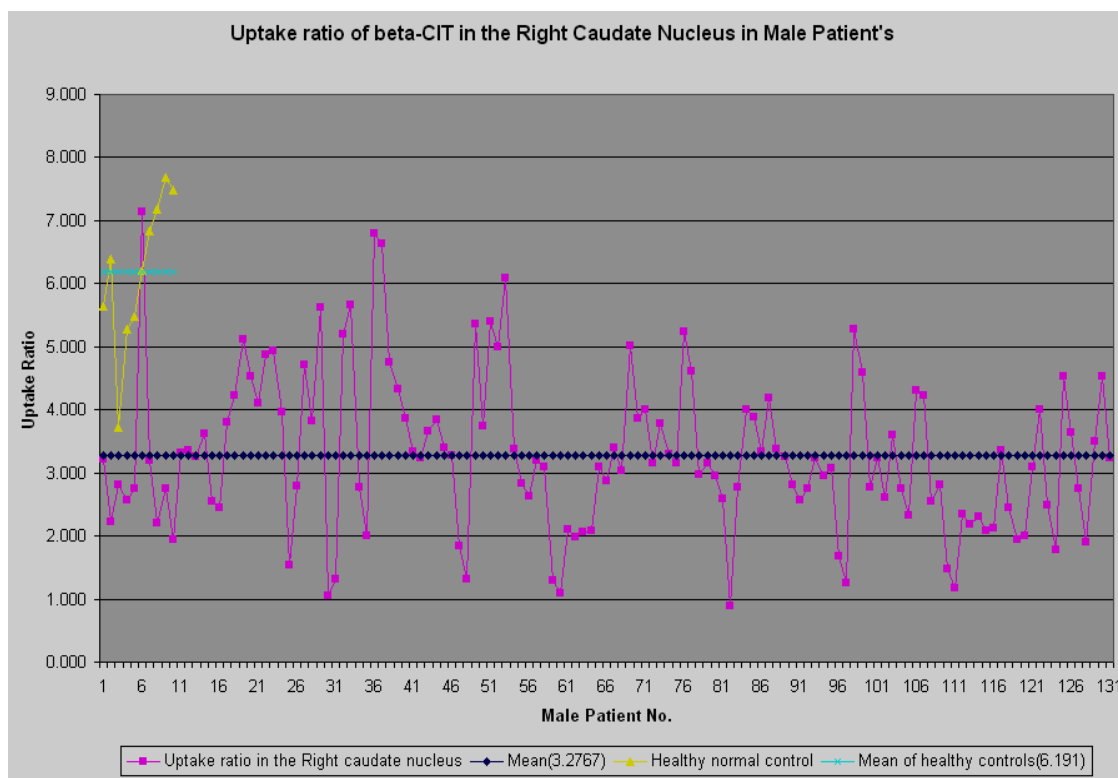

Figure 3.11 Uptake Ratio of beta-CIT in Right Caudate Nucleus of 42 Female patients. The Blue color plot is for the mean uptake ratio of 42 female patients, Pink color is for uptake ratios of each female patient and the yellow color is for the uptake ratio of 10 normal healthy control subjects. The mean uptake ratio for 42 Female patients is **3.93**. The mean uptake ratio for healthy control is **6.19**.

From the Figure 3.10 and Figure 3.11 the mean of the uptake ratios in the Right Caudate Nucleus of male patients is 3.28 and that in female patients is 3.93 respectively. The mean of the uptake ratio for 10 healthy controls is 6.19. Of the 10 healthy normal control subjects one subject has very low value of uptake ratio which is comparable to the uptake ratio of the patient. From Figure 3.10 it can be seen that one

of the male patient's has very high value of uptake ratio which is comparable to the uptake ratio of a normal healthy control. This patient could be very young as compared to the other patients'. From the plots it is also seen that the mean uptake ratio of male and female patients' is less than the mean uptake ratio in healthy controls.
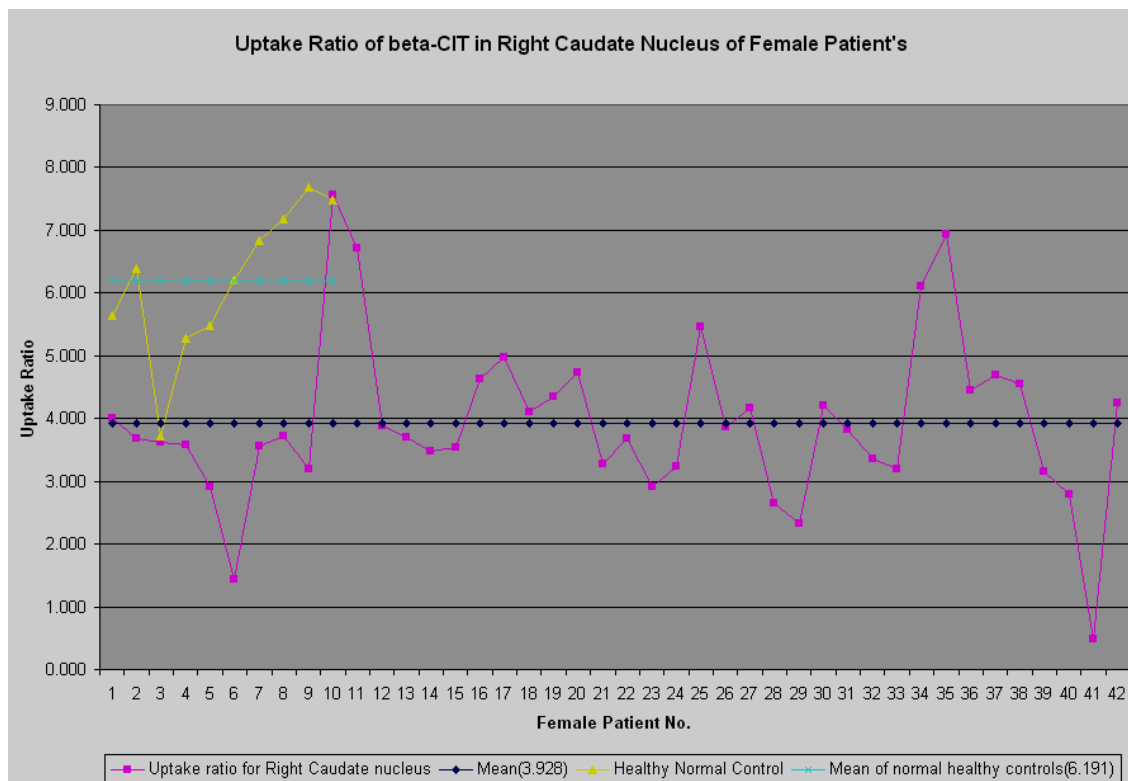

Figure 3.12 Uptake Ratio of beta-CIT in Right Anterior Putamen of 131 male patients. The Blue color plot is for the mean uptake ratio of 131 male patients, Pink color plot is for uptake ratios of each male patient, the green color plot is for the mean uptake ratio for 10 healthy controls and the yellow color plot is for the uptake ratio of 10 normal healthy control subjects. The mean uptake ratio for 131 male patients is **3.23.** The mean uptake ratio for healthy controls is **6.10**.

From Figure 3.12 mean uptake ratio of male patients' is 3.23 and the mean uptake ratio in 10 normal healthy controls is 6.10. Even here there is a vast difference in the uptake ratios in 131 male patients.

52

Figure 3.13 Uptake Ratio of beta-CIT in Right Anterior Putamen of 42 Female patients. The Blue color plot is for the mean uptake ratio of 42 female patients, Pink color plot is for uptake ratios of each male patient, the green color plot is for the mean uptake ratio for 10 healthy controls and the yellow color is for the uptake ratio of 10 normal healthy control subjects. The mean uptake ratio for 42 female patients is **3.83**. The mean uptake ratio for healthy control is **6.10**.

The Figures 3.13 above shows that the mean uptake ratio for healthy controls is 6.10 and the mean uptake ratio for 42 female patients is 3.83. There is a lot of variation in the uptake ratios of the female patients'.
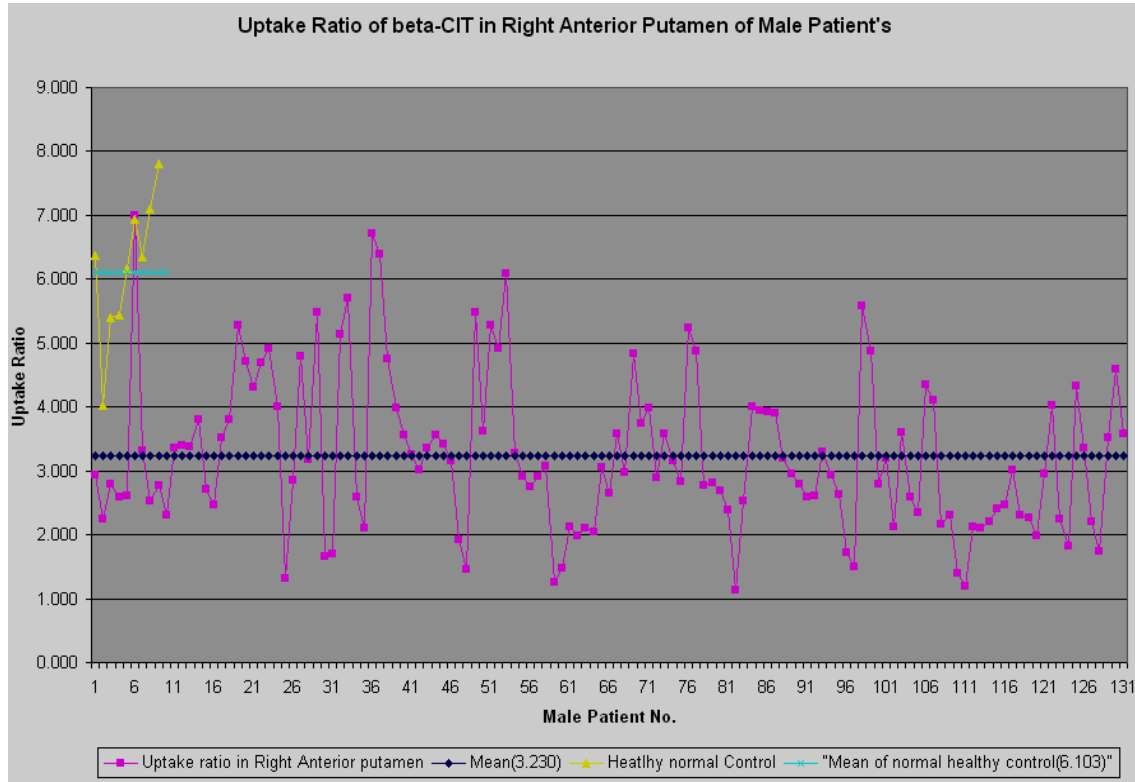
Figure 3.14 Uptake Ratio of beta-CIT in Right Posterior Putamen of 131 male patients. The Blue color plot is for the mean uptake ratio of 131 male patients, Pink color plot is for uptake ratios of each male patient, the green color plot is for the mean uptake ratio for 10 healthy controls and the yellow color plot is for the uptake ratio of 10 normal healthy control subjects. The mean uptake ratio for 131 male patients is **2.04**. The mean uptake ratio for healthy controls is **4.84**.

Figure 3.14 depicts the mean uptake ratio of right posterior putamen in 131 male patients is 2.04 and the mean uptake ratio of 10 healthy controls is 4.84.
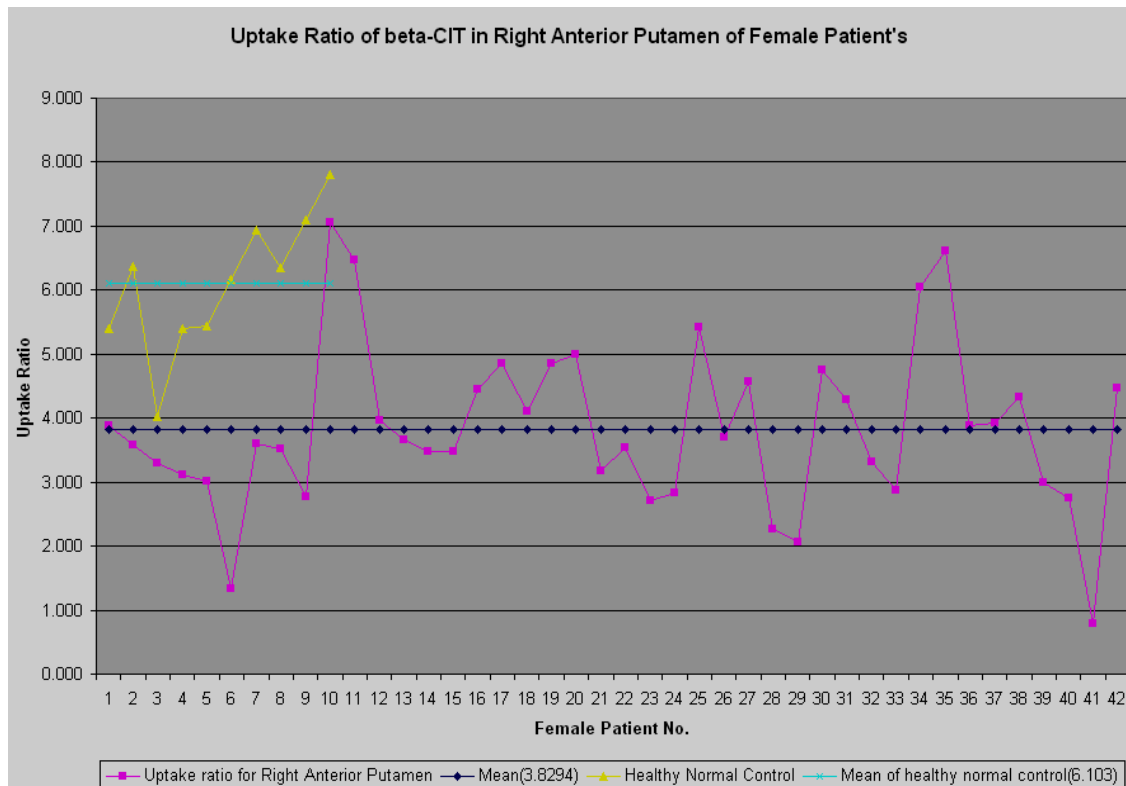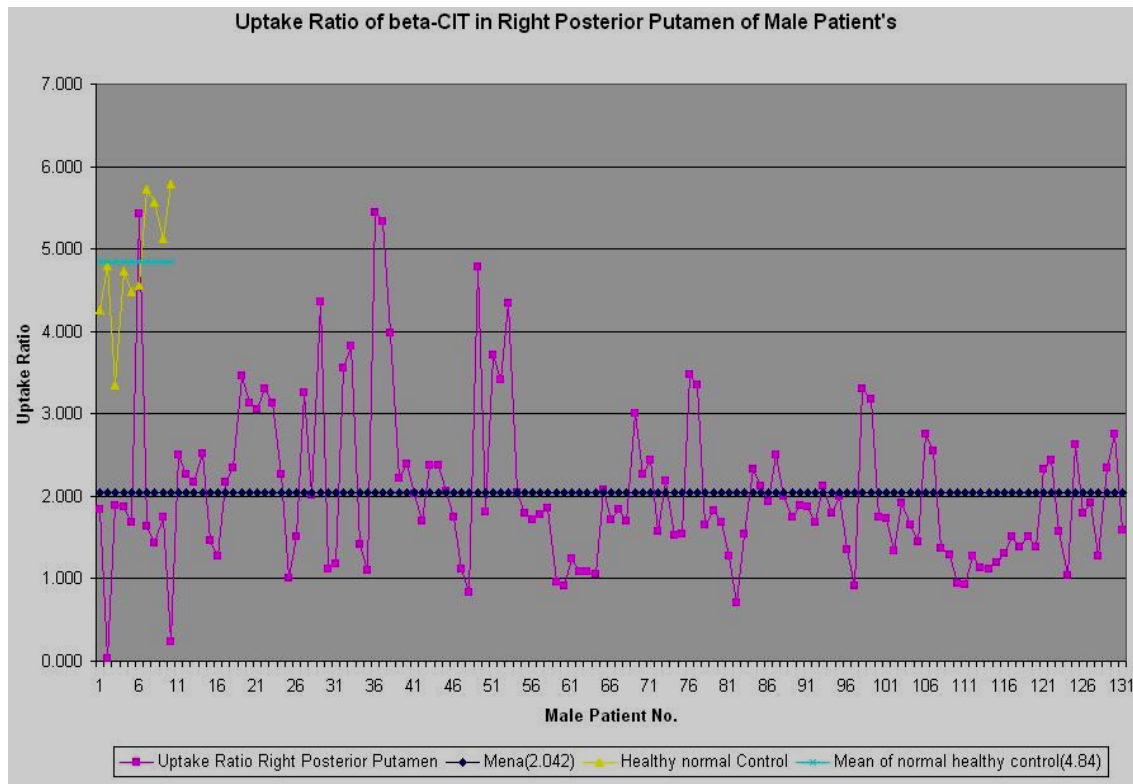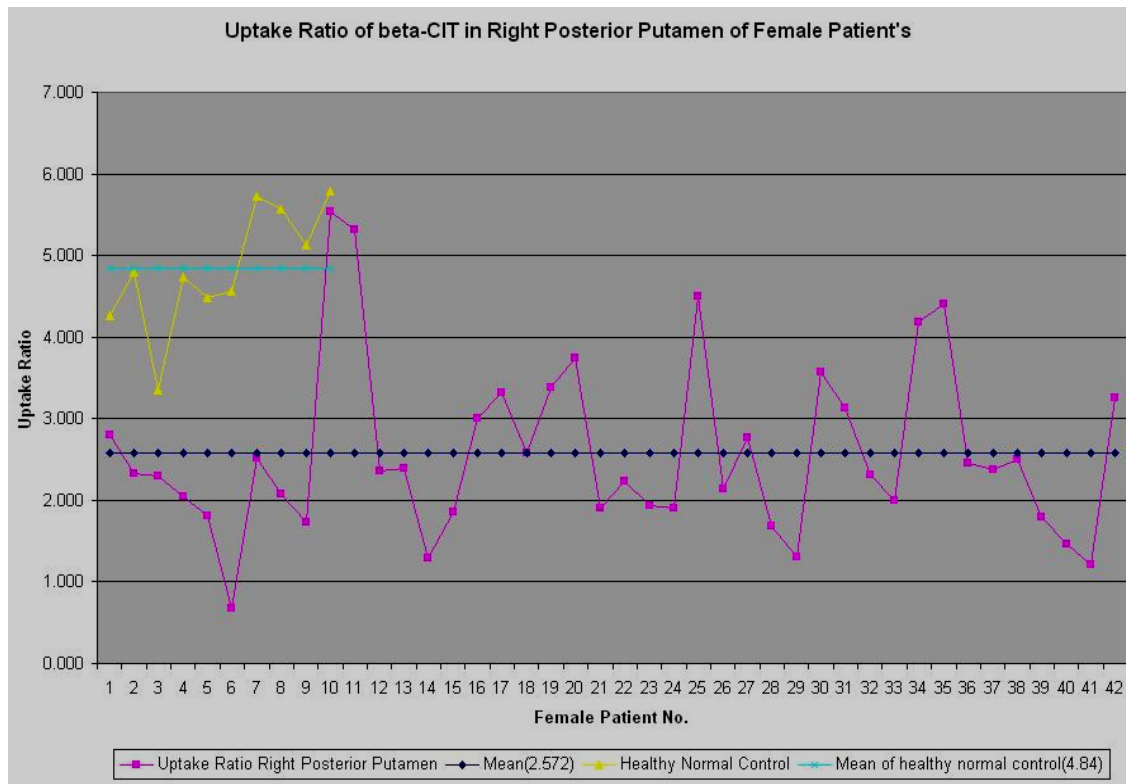
Figure 3.15 Uptake Ratio of beta-CIT in Left Posterior Putamen of 42 Female patients. The Blue color plot is for the mean uptake ratio of 42 female patients, Pink color plot is for uptake ratios of each female patient, the green color plot is for the mean uptake ratio for 10 healthy controls and the yellow color is for the uptake ratio of 10 normal healthy control subjects. The mean uptake ratio for 42 female patients is **2.57**. The mean uptake ratio for healthy control is **4.84**.

Form the Figure 3.15 the mean uptake ratio of in the right posterior putamen of 42 female patients' is 2.57 and the mean uptake ratio for the same VOI for the healthy controls is 4.84. The vast difference in the uptake ratios of the female patients' could be because of the vast difference in their age groups.

From the previous studies it has been demonstrated that uptake ratios of different VOIs are not gender biased. From the Table 3.3, the means of the uptake ratios in right sided VOIs of the male and female patient's are approximately in the same

55

range. To determine whether the mean uptake ratios were equivalent a T-test was calculated with the alpha value set at 0.01. The T-test results are displayed below.

Table 3.4 Illustrates the results of the T-test performed on the mean and variance of the uptake ratios in the right sided VOIs of 131 male patient's and 42 female patients'.

alpha value is 0.01						
T-test	RightCaud	RightANTPUT	RightPOSTPUT	LeftCaud	LeftANTPUT	LeftPOSTPUT
P-value	0.0060	0.0101	0.0058	0.0501	0.1168	0.1183

From the Table 3.4, the P-values for the Right side of the VOIs are less than the alpha value and the P-values of the left side of the VOIs are more than the alpha value. So for the right sided VOIs the mean of the uptake ratios across the male and the female patient's is different and for the Left sided VOIs the mean of the uptake ratios across the male and the female patient's is the same. These results mean that the uptake of [^{123}I] β-CIT on the right side of striatal regions such as caudate nucleus, anterior putamen and posterior putamen of the same patients' is more significant than that on the left side. This is inconsistent with the findings from the previous studies. Also there is a vast variation in the uptake ratios for the male and female patient's for all the VOIs. One reason behind this could be the age difference in the normal healthy subjects. The patient who has very low value of uptake ratio could be older as compared to other normal healthy controls. For this study age of the patients' was not provided.

Next the results obtained from this approach are discussed. The discussion provides some suggestions to provide better results, and provide insight for more studies that can be performed with this approach.

3.2 Discussion

Imaging of the presynaptic DAT has evolved into an important diagnostic tool for patients with parkinsonian syndromes [10, 11]. In many cases, visual assessment of DAT SPECT studies enables clinicians to decide whether neurodegeneration of presynaptic neurons has occurred or to confirm and exclude a neurodegenerative parkinsonian syndrome [12]. However, for early diagnosis, the detection of critical changes in DAT binding in subregions is critical, as it is as well for monitoring disease progression to investigate the effects of putative neuroprotective drugs, and thus quantitative measures are essential.

Previous work has demonstrated significant decrease of DAT in striatal regions using SPECT radio ligand [123I] β-CIT. In most of these studies, analyses were done based on the ratio of specific to non-specific striatal [123I] β-CIT binding, which is calculated by dividing the specific striatal uptake by the occipital uptake. According to Pirker and Susanne Asenbaum et al the counts in striatal regions were calculated on consecutive slices which were 3.5 mm thick and the slices with highest counts were used. Irregular ROIs were drawn in areas corresponding to the left and right striatum and occipital cortex with the help of a brain atlas by a single examiner. Values of non-specific binding (cerebellar region) was calculated by overlaying two cerebellar ROIs in

57

three consecutive axial slices and pooling out the cerebellar counts. The ratio of striatum/cerebellum -1 represents the specific to non specific striatal binding. Studies performed by [Winogrodzka et al. and Van Royen et al.] shows that the ratio of specific to non–specific binding was calculated by summing two transversal slices representing the most intense striatal binding. A standard region of interest (ROIs) template was constructed according to the stereotactic atlas and including the fixed regions for putamen, caudate nucleus and occipital regions. This template was placed bilaterally over the image. The estimates of specific striatal binding were made by subtracting occipital counts from total striatal counts. The ratio of specific to non-specific striatal [^{123}I] β-CIT binding was then calculated by dividing the specific striatal uptake by the occipital uptake. G. Tissingh et al. and P. Bergmans et al. used a similar technique to as used by Winogrodzka et al. and Van Royen et al. to calculate the specific to non-specific striatal [^{123}I] β-CIT binding. In the present study VOIs were created from the MRI images and the SPECT images, thus matching the functional counts and the anatomical counts. The patient's images were registered with the tracer specific template. And 3-D overlap of the VOIs over the patients' images was performed. Thus, the analyses were done based on the volumes of the striatal regions such as caudate nucleus and putamen. Earlier studies [6, 9, and 21] proved that the putamenal binding of [^{123}I] β-CIT is lower than that in caudate nucleus. But not a single study demonstrated dividing the putamen region into anterior and posterior sub-regions to perform the analyses. In the present study, the sub-regions of the putamen were separately analyzed to specify exactly which area of the putamen has lower binding.

Therefore, to address the limitations of existing quantitation techniques here the analyses is done by overlapping the VOIs and not the ROIs over the patient's images and then calculating the specific to non-specific [123I] β-CIT binding in the striatal regions. Many functional brain imaging analyses begins with registration of subject images to a template of healthy normal control subjects. This template can be either general template provided by SPM or a tracer-specific template. Here a tracer-specific template was developed to analyze the patients' which are administered with the drug containing [123I] β-CIT. If the SPM generated template was used or any other radio tracer template had been used then not much information would have been available because of errors in registration as well as improper match of spatial resolution.

Based on the T-test performed it was shown that the mean uptake ratio of different VOIs for male and female are not same. For this work the only patient demographic provided was gender. Earlier studies suggest that the uptake ratio is not gender biased [2, 3, and 9]. But from this study there is difference in uptake ratio across male and female. This difference is illustrated by the plots in results section above. But this finding can be related to earlier studies findings if the age information of the patients was also provided. The DAT degeneration is prominent in elder normal controls than in the younger normal controls. So, it could be possible that patients in this study were from different age groups. And because of patients from different age groups there is a difference in mean uptake ratio between male and female patients.

Ten normal healthy controls were recruited for this study, from which the template was created. A more standard and stable VOI can be created from a larger

number of controls. By using a template created from the healthy controls the PD patients' did not require the MRI images, as the PD patients' can be spatially normalized using the template. So, if a large number of controls is available then an average template will represented by a large group. This will contribute more accuracy towards the spatial normalization of the PD patient's. A larger number of healthy normal controls would also allow researchers to examine the ability of [^{123}I] β-CIT SPECT to aid in the discrimination of patients with early PD from healthy controls, and to investigate the relationship between the binding measures. With further calculation based on the binding potential discrimination between early and late PD patients is possible [3, 6]. The binding potential can also depict that the binding in the putamen is lower than in the caudate nucleus, in both early and late PD patients, in contrast to equal putamen and caudate nucleus binding in ten healthy controls [7].

CHAPTER 4

CONCLUSION

4.1 Conclusion

A method for quantification of in vivo binding of radiotracer by the specific (striatum)-to-non-specific (occipital lobe or cerebellum) uptake ratio as to determine binding potential was performed. The [^{123}I] β-CIT SECT images have little specific binding. Because of this little specific binding the brain boundaries are not distinguished. But in the present study in spite of the little specific binding, the results provide a decent measurement of the [^{123}I] β-CIT binding in the striatal regions. This technique performs the VOI analyses and provides detail measure about the DAT degeneration in early PD.

There is ongoing progress in the optimization of radioligands for components of the dopaminergic neurotransmission system. These techniques will also be used in clinical trials to evaluate neuroprotective properties of drugs in patients with Parkinson's disease.

APPENDIX A

ELIMINATING FIDUCIAL MARKERS
(USING MRIcro)

APPENDIX A. ELIMINATING FIDUCIAL MARKERS

1.The reconstructed SPECT images are treated for fiducial markers, by using MRIcro

2.A boundary is drawn around the fiducial markers using drawing tool of MRIcro.

3.Once the boundary is drawn around a region, the region is selected by filling the

region.

4. The selected region is now deleted by using a "Delete regions with ROI tool" from
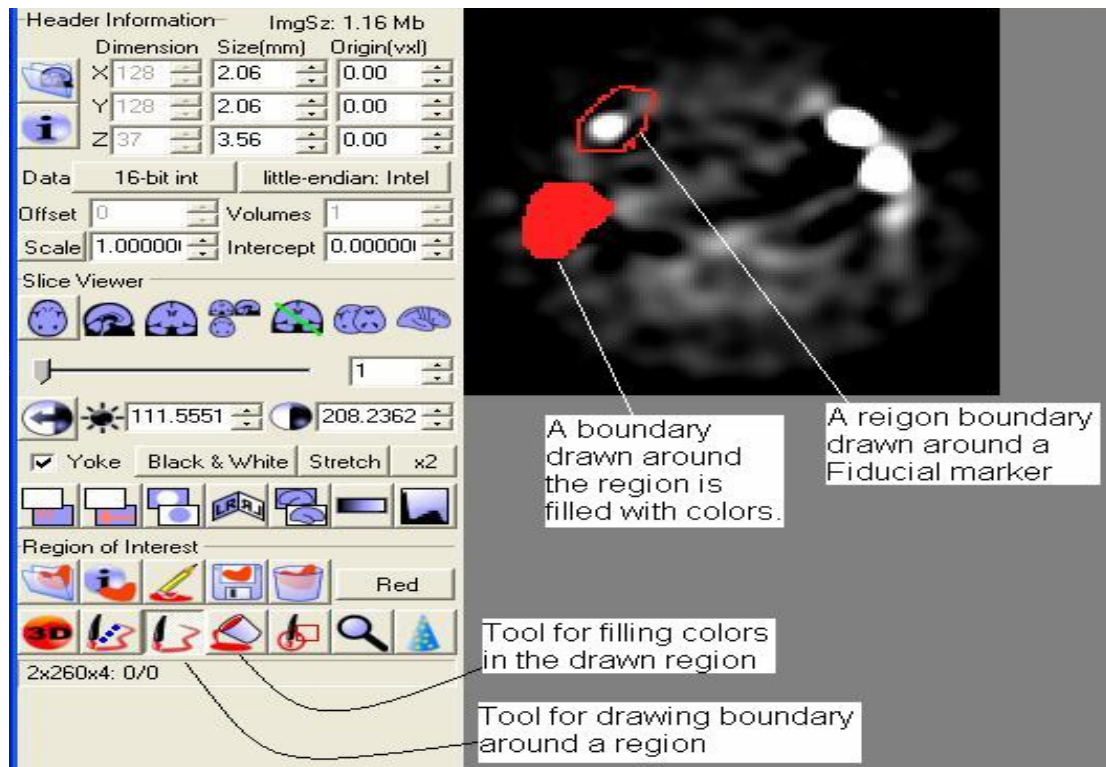
the ROI tool bar.

Figure A.1 The use of MRIcro drawing tools, using this tool a boundary is drawn around a region to be deleted
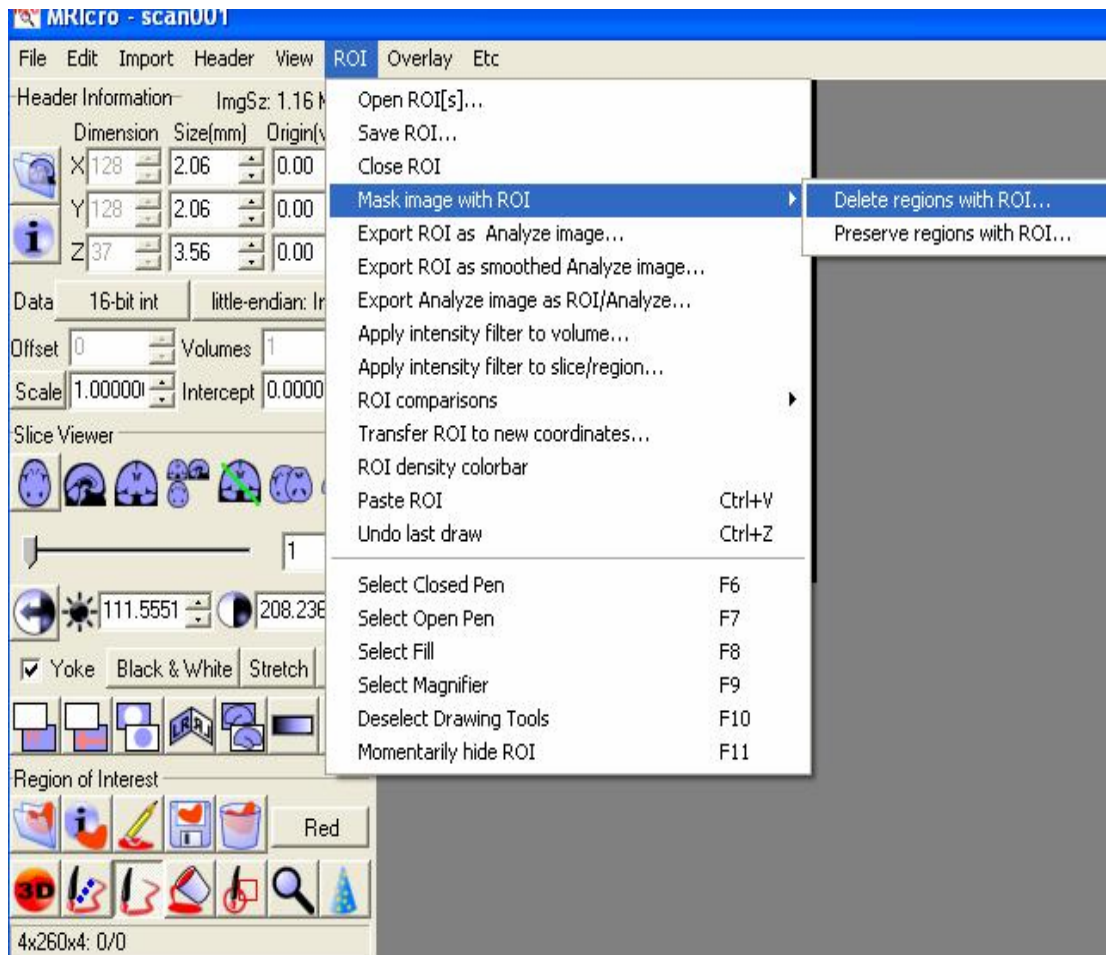
Figure A.2 The tool in MRIcro used to delete the drawn regions.

APPENDIX B

CO-REGISTRATION AND SPATIAL NORMALIZATION

OF WITHIN MODALITY CROSS MODALITY IMAGES

(SOFTWARE USED SPM)

APPENDIX B
CO-REGISTRATION AND SPATIAL NORMALIZATION
OF WITHIN MODALITY CROSS MODALITY IMAGES
(SOFTWARE USED SPM)

1) For the Co-registration and Spatial Normalization certain parameters are need to be chosen based on which the registration is performed.

2) By using the utilities select the suitable working directory from which the images to be processed can be easily imported and stored.

3) Click on "Defaults". A drop down menu will appear in which an action to be performed is selected.

    a) If spatial normalization is selected the second drop down menu will appear where in one has to choose one of the two options "Write normalized" or "Parameter Estimation".

        i) The "Parameter for Estimation" will provide a choice for performing the registration such as "Weight template when registering", then "Weight source images when registering", then to select the cutoff, then to select the regularization, then to select the type of iterations "non-linear" or "linear".

        ii) If the "Write Normalized" option is selected, then it will provide the option to "Preserve Concentration", then an option to select the bounding box will appear For this study a "Template[-90:90, 126:90 -72:108]" was selected. Then option to select the voxel size will appear for this study the voxel size was selected.

4) Then an option to choose the interpolation technique will appear, in here an "A Tri-linear interpolation was selected". After these settings the "Normalize" function was executed. Again it will ask an option to select the "Determine parameters and write

normalize". Once this option is selected a window will pop up asking for the template image. In the present study, T1 MNC is used as a template image. Then SPM provide an option to select the Source image, here the MRI image of the normal healthy control is selected. After that the Image to write was the SPECT image to which is supposed to be normalized to the standard stereotactic atlas. Spatial normalization registers the images across modality as well as across subjects.

a. Once you select the co-registration you will be provided an option to select the "cost function". The recommended cost function is "Mutual Information". Then an option to choose the interpolation method is provided, the recommended is Tri-linear interpolation. Then an option to choose the "wrap" method is provided, the recommended is not to wrap. Then a choice to "Mask" was provided. The recommended is "don't mask". Once these setting are chosen, the co-registration function can be executed from the GUI. The function will ask to input the no. of images and then it will ask to choose the option to "co-register or re-slice". Once these parameters are chosen then a window will appear where you can navigate through different folders ad choose the "Target Image".

b. In this study the MRI image of the healthy control was chosen as a target image. Then an image to write is select as the SPECT image of the healthy normal control. By executing this function. The SPECT image of the healthy control is converted to the MRI space. So, the co-registration is chosen to register the images across the modality but of the same subject. The spatial

normalization stores the image with prefix "w" in the working directory in the analyze format. The co-registration stores an image with prefix 'r' in the working directory in the analyze format.

The figure below displays the SPM2 interface by using which the function of spatial normalization and co-registration was executed.
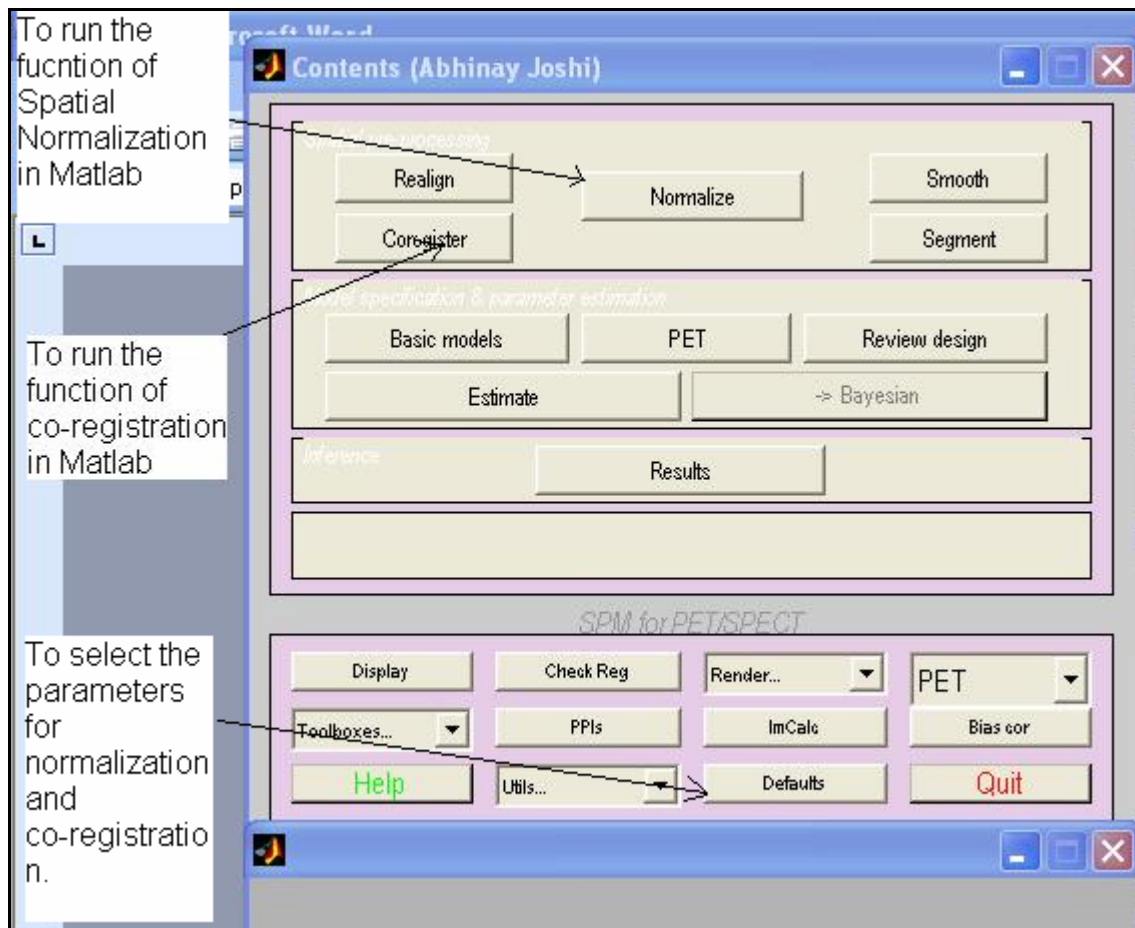

Figure A.3 To run the co-registration and spatial normalization function in MATLAB, the functions shown in the GUI were used.

APPENDIX C

COUNT NORMALIZATION

APPENDIX C COUNT NORMALIZATION

1) The function "SPM_adjmean_ui" is executed in the MATLAB to perform count normalization. Once the function is executed the GUI will provide an option to choose images. Once the images are chosen, the number of images to be count normalized needed to be specified in SPM. The Figure 5 illustrates this method.
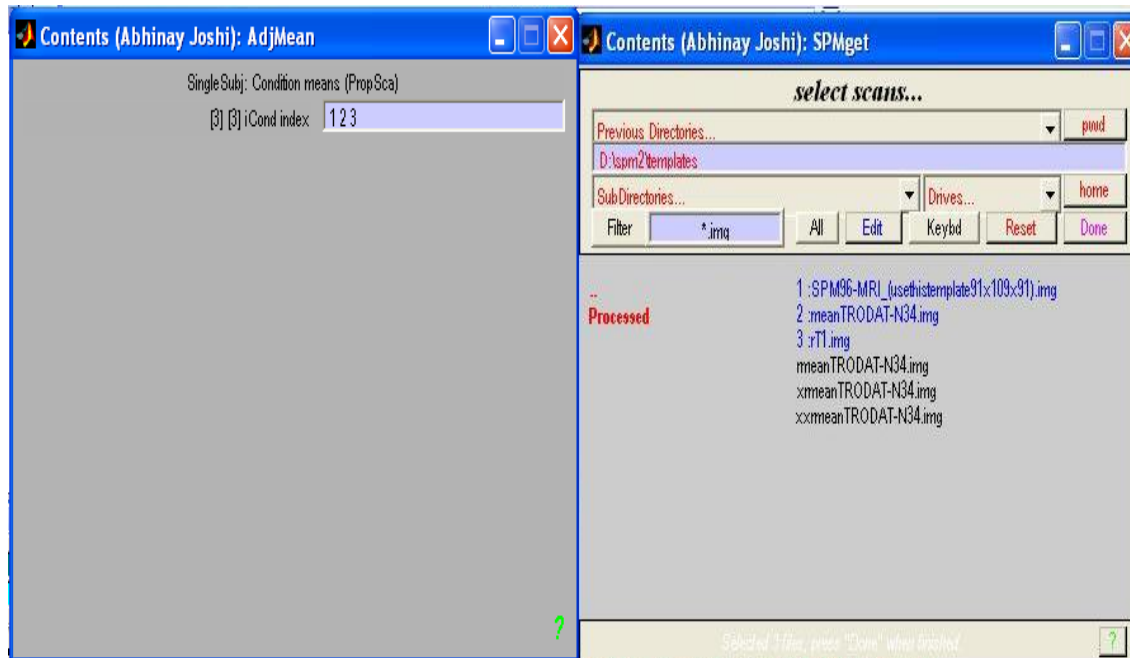

Figure A.4 The figure shows the way in which images to be count normalized are chosen in the SPM. The count normalized image is stored in the working directory in the ANALYZE format.

2) The intensity counts of a SPECT scan changes based on the on the injected amount of the dose as well as the timing of the dose. The count normalization adjusts the intensity counts, by averaging the intensity counts in a scan using all the locations in the entire "bounding box" which cover the entire head. In other word this technique brings the contrast and the brightness of the scan to a comparable magnitude. Count

normalization provides a choice to save the image with the name of our choice in analyze format.

APPENDIX D

AVERAGING

APPENDIX D AVERAGING

1) The images are averaged by executing the function "imcalc" from the SPM GUI. The mean of all the images is calculated. Just like for the count normalization the SPM tool for averaging will ask for more than one image for averaging, if more than one image is not provided the function will not execute. The number of the images to be averaged is chosen in the window that appears in the SPM interface. Once the images are chosen, a window will appear where we have to enter the illustration,

$$\frac{(i1 + i2 + i3 + ... + in)}{n} \text{-----------------------------}1$$

2) Once this illustration is entered in the field SPM takes some couple of minutes based on the number of images to give an average image. This image is stored in the Analyzed format in the working directory with the name of our choice.

REFERENCES

[1] Walter Pirker, Susanne Asenbaum, Martin Hauk, Susanne Kandlhofer, Johannes Tauscher, Matthaus Willeit, Alexander Neumeister, Nicole Praschak-Reider, Peter Angelberger and Thomas Brucke, "Imaging Serotonin and Dopamine Transporters with ^{123}I-β-CIT SPECT: Binding Kinetics and Effects of Normal Aging", The Journal of Nuclear Medicine, Vol. 41, No. 1, January 2000

[2] Jan Booij, Gerrit Tissingh, Ania Winogrodzka, Eric A. van Royen., "Imaging of the dopaminergic neurotransmission system using single-photon emission tomography and positron emission tomography in patients with parkinsonism, Europen Journal of Nuclear Medicine, Vol. 26, No. 2, February 1999.

[3] Caroline Pruiner, MD; Pierre Payoux MD; Denis Guilloteau, PhD; Sylvie Chalon; Bruno Giraudeau, PhD; Cynthia Majorel, PhD; Mathieu Tafani, PhD; Erwan Bezard, PhD; Jean-Paul Esquerre, PhD; and Jean –Louis Baulieu, PhD, "Quantification of Dopamine Transporters by ^{123}I-PE2I SPECT and the Non-invasive Logan Graphical Method in Parkinson's Disease", The Journal of Nuclear Medicine, Vol. 44, No. 5, May 2003

[4] http://www.parkinson.org

[5] Kim A. Bergstrom, Erkki Tupala and Jari Tiihonen , "Dopamine Transporter in vitro Binding and in vivo Imaging in the Brain", Pharmacology and Toxicology, 88, 287-293,2001

[6] G. Tissingh, P.Bergmans, J.Booij, A. Winogrodzka, E.A. Van Royen, J.C. Stoof, E.C. Wolters, "Drug-naïve patients with Parkinson's disease in Hoehn and Yahr stages I and II show a bilateral decrease in striatal dopamine transporters as revealed by [^{123}I] β-CIT SPECT", Journal of Neurology, 245, Pg. 14-2,1998

[7] Nora D. Volkow, Joanna S. Flower, S. John Gately, Jean Logan, Gene-Jack Wang,-Shin Ding and Stephen Dewey, "PET Evaluation of the Dopamine Syatem of the Human Brain", The Journal Of Nuclear Medicine, Vol. 37, No. 7, July 1996

[8] R.J. Vermeulen, E.Ch. Wolters, G. Tissingh, J. Booij, A.G.M. Janssen, J. Habraken, E. Sokole-Busemann, J.C. Stoof and E.A. Van Royen, "Evaluation of [^{123}I] β-CIT Binding with SPECT in Controls, Early and Late Parkinson's disease", Nuclear Medicine Biology, Vol. 22, No. 8, pp 985-991,1993

[9] Ali A. Bonab, Alan J. Fischman, and Nathaniel M. Alpert, "Comparison of 4 Methods for the Quantification of Dopamine Transporters by SPECT with [^{123}I] IACFT", The Journal of Nuclear Medicine, Vol. 41, No. 6, June 2000

[10]   E. Watanabe, Y. Mayanagi, Y. Kosugi, S. Manaka and K. Takakura, "Open Surgery by the Neuronavigator, a stereotactic, articulated, sensitive arm", Neurosurgery, vol. 28, No. 6, pp. 792-799, 1991.

[11]   R. L. Galloway, C.A. Edwards, J.T. Lewis, and R. J. Maciunas, "Image display and surgical visualization in interactive image-guided surgery", Optical Engineering, vol. 32. No. 8, pp. 1955-1962, 1993.

[12]   Hagen Schiffbauer, "Neuronavigation in Brain Tumor Surgery", Department of Neurosurgery, Oulu 1999.

[13]   Barbara Zitova, Jan Flusse, "Image Registration methods: a survey", Image and Vision Computing, vol. 21, pp.977-1000, 2003.

[14]   Jeongate Kim, Jeffery A. Fessler, "Intensity-based Image Registration using Robust Correlation Coefficients", IEEE TRANSACTIONS ON MEDICAL IMAGING, vol. 23 No. 11, pp. 1430-1444, November 2004.

[15]   Karin Kneőaurek, Marija Ivanovic, David A. Weber,"Medical Image Registration", Europhysics News, vol. 31, No. 4.

[16]   Karl J. Friston, "Introduction: Experimental Design and Statistical Parametric Mapping", The Wellcome Department of Cognitive neurology, University College London.

[17]   Booij J, Speelman JD, Horstink MW, Wolters EC, " The clinical benefit of imaging striatal dopamine transporters with [123I]FP-CIT SPET in differentiating patients with presynaptic parkinsonism from those with other forms of parkinsonism. European Journal of Nuclear Medicine, vol. 28, 266-272, 2001.

[18]   Benamer TS, Patterson J, Grosset DG, "Accurate differentiation of parkinsonism and essential tremor using visual assessment of [123I]-FP-CIT SPECT imaging: The [123I]-FP-CIT Study Group. Moving Disorder, vol. 15, 503-510, 2000.

[19]   A Winogrodzka, P Bergmans, J Booij, E A van Royen, J C Stoof, E C Wolters, "[123I] β-CIT SPECT a useful method for monitoring dopaminergic degeneration in early stage Parkinson's disease", Journal of Neural Neurosurg Psychiatry, vol. 74, pp. 295-298,2003.

[20]   Seibyl J.P., Marek K., Sheff K., Zogbi S., Baldwin R. M., Charney D. S., Van Dyke C. H., Innis R. B., "Iodine-123-beta-CIT and Iodine-123-FPCIT SPECT measurement of dopamine transporters in healthy subjects and Parkinson's patients, "Journal Nuclear Medicine, vol. 39(9), pp.1500-1508, September 1998.

[21]   Walter Pirker, Schiva Djamshidian, Susanne Asenbaum, Willibald Gerschlager, Gotthard Tribl, Martha Hoffman and Thomas Brucke, "Progression of Dopaminergic Degeneration in Parkinson's Disease and Atypical Parkinsonism: A longitudinal β-CIT SPECT study", Movement Disorders, vol. 17, No.1, pp. 45-53, 2002.

BIOGRAPHICAL INFORMATION

Abhinay Joshi received his Bachelor of Engineering degree in Instrumentation Engineering from Mumbai University in 2002. He then worked for TATA CONSULTANCY SERVICES, India as a system and design engineer. He started his masters in Biomedical Engineering at The University of Texas at Arlington in 2003. Due to his interests in Medical Imaging and Image Processing, he started working on research projects involved in Registration of Functional Brain Images with Dr. Michael D. Devous, Sr. He worked as an Intern at the University of Texas Southwestern Medical Center Dallas in summer 2005. Being interested in the field of Medical Imaging he started working as a Graduate Research Assistant on Registration of β-CIT Dopamine Transporters SPECT images and pursued a thesis in that topic.